DVB-T based Passive Bistatic Radar

Jonas Myhre Christiansen

Norwegian Defence Research Establishment (FFI)

8 June 2010

Keywords

Radar

Passiv bistatisk radar

Digital TV

Approved by

Uta Gjertsen	Project Manager
Vidar S. Andersen	Director

English summary

The interest for bi- and multistatic radar systems has gone in cycles of approximately 15 years. Currently we are at the peak of such a cycle, which mainly is driven by the interest for Passive Bistatic Radar systems. The most well-known Passive Bistatic Radar systems are Silent Sentry 3 developed by Lockheed Martin, and the Home Alerter 100 developed by Thales.

Passive Bistatic Radar systems offer covert air surveillance at a potentially low cost. However, the emerging systems Silent Sentry 3 and Home Alerter 100 are based on FM-radio transmitters of opportunity, where the main drawback is the relatively low bandwidth, resulting in poor range resolution. The long integration time yields fine Doppler resolution. The next generation Passive Bistatic Radar systems will be based on digital transmitters like the Digital Video Broadcast - Terrestrial signals. These systems will not have the range resolution problem, but rather be facing the situation of targets moving through both range and Doppler bins during the system's signal integration time.

Long integration time gives fine Doppler resolution, and problems due to Doppler walk may arise. The relatively high bandwidth of the Digital Video Broadcast - Terrestrial signal gives fine range resolution, and problems due to range walk may arise. These problems have been analyzed in this work, with both simulated and experimental data. Range walk is shown to cause problems for targets having normal velocity and maneuverability, i.e. sub sound velocity aircrafts. Loss of target signal-to-noise ratio when using long integration times were demonstrated by simulations and real life data processing. Doppler walk was shown to be a more rare phenomenon, mostly due to the low maneuverability and speed of the targets of opportunity. However, in the simulated case, Doppler walk of high bistatic accelerated targets is shown.

In order to compensate for the range walk, a method to lower the effects of range walk is studied. The method is based on the Doppler information in the Doppler-delay processing. An adaptive processing scheme is proposed, and the advantages and disadvantages are discussed.

Sammendrag

Interessen for bi- og multistatiske radarsystemer har gått i sykler på ca. 15 år. Interessen er for øyeblikket på topp hovedsaklig drevet av interressen for Passive Bistatic Radar systemer. De mest kjente Passive Bistatic Radar systemene er Silent Sentry 3 utviklet av Lockheed Martin, og Home Alerter 100 utviklet av Thales.

Passive Bistatic Radar systemer har mulighet for skjult luftovervåking til en potensielt lav kostnad. Systemer som Silent Sentry 3 og Home Alerter 100 er basert på bruk av FM sendere, hvor hovedulempen er lav båndbredde som gir en dårlig avstandsoppløsning. Den lange integrasjonstiden gir en god Doppler-oppløsning. Den neste generasjon Passive Bistatic Radar systemer, basert på digitale sendere slik som Digital Video Broadcast - Terrestrial har ikke problemet med avstandsoppløsning, men vil heller ha tilfeller hvor målet går gjennom flere avstands- eller Doppler-celler i integrasjonsintervallet.

Lang integrasjonstid gir liten Doppler-oppløsning, og problemer grunnet Doppler-spredning kan oppstå. Den relativt høye båndbredden i Digital Video Broadcast - Terrestrial systemet gir lav avstandsoppløsning, og problemer grunnet avstandspredning kan oppstå. I dette arbeidet har problemene blitt analysert med både simulerte og eksperimentelle data. Avstandspredning skaper problemer for mål med normal hastighet og manøvrerbarhet, mao. fly med underlydshastighet. Tap av signal til støy forhold ved bruk av lange integrasjonsintervaller er demonstrert med både simuleringer og eksperimentelle data. Doppler-spredning er ett sjeldnere fenomen, mest grunnet lav manøvrerbarhet og hastighet for målene. I simuleringer er Doppler-spredning for mål med høy bistatisk akselerasjon vist.

En metode for å kompensere for avstandspredning er analysert. Denne metoden bruker Doppler-informasjon i Doppler-delay prosesseringen. Et adaptivt proseeseringskjema er foreslått, samt fordeler og ulemper er diskutert.

Contents

Introduction

The interest for bi- and multistatic radar systems has gone in cycles of approximately 15 years. Currently we are at the peak of a cycle, which mainly is driven by the interest for PCL (Passive Coherent Location) systems. The most well-known PCL systems are Silent Sentry 3 (SS3) developed by Lockheed Martin, and the Home Alerter 100 (HA100) developed by Thales.

PBR (Passive Bistatic Radar) systems offer covert air surveillance at potentially low cost. However, the emerging systems SS3 and HA100 are based on FM (Frequency Modulation) - radio transmitters of opportunity, where the main drawback is the relatively low bandwidth, resulting in poor range resolution, while having fine Doppler resolution. The next generation PCL systems, based on digital transmitters like the DVB-T (Digital Video Broadcast - Terrestrial) signals will not have the range resolution problem, but rather be facing the situation of targets moving through the range and Doppler bins during the system's signal integration time.

PBR, defined as "Exploiting commercial broadcast transmitters for bistatic and multistatic operation" [8], p 28-29, can be regarded as a subset of the larger group of PCL systems. This work will analyze a DVB-T based PBR system, with an emphasis on the potential problems of range and Doppler walk. Range walk is defined as when the target moves through one or more range bins during integration, and Doppler walk is defined as when the target moves through one or more Doppler bins during integration.

The first part of this work presents the theory. The basic bistatic radar theory is presented, and the differences between monostatic and bistatic radar is emphasized. The DVB-T signal waveform and properties is studied, with an emphasis on the usage as a radar waveform. The radar processing technique used is explained, which uses the Ambiguity Function. Range and Doppler walk is explained, and a mathematical estimate of occurrence of range and Doppler walk is developed. And finally, the simulator and experimental hardware, which generate simulated and real data is described.

The second part of this work consists of an analysis of the simulated and experimental data. Range and Doppler walk are analyzed, and their effects on target S/N are described. Finally, a possible solution to minimize the effects of range walk is analyzed, and the advantages and disadvantages are discussed.

1 Bistatic Radar

Bistatic radar is a radar with transmitter and receiver spatially separated. As seen in [7], there exists no unambiguous definition of bistatic radar. The development of bistatic radar has gone through cycles of approximately 15 years [3], and we are now at the peak of a cycle driven by PCL/PBR systems.

PCL systems can be regarded as a collection of individual PBR systems using the same multichannel receiver. Therefore, bistatic theory which will be presented in this section applies in a high degree to PCL/PBR systems. All bistatic theory applies to PBR systems with the transmitter as a non-cooperative illuminator. And all bistatic theory applies to monostatic radar by setting the bistatic angle $\beta = 0$ and $L = 0$.

Bistatic radar has the following advantages:

- covert operation of receiver (because it is passive, i.e. it sends out no signals in the radar frequency domain).

- better protection against jamming and other electronic countermeasures.

- higher chance of detecting stealth vehicles

Disadvantages of bistatic radar:

- complex geometry and processing.

- communication between sites.

- more elements to deploy.

- reduced low level coverage because of needed line of sight from several locations.

1.1 Bistatic Geometry

The bistatic geometry is illustrated in figure 1.1. The geometry is based on the separation of transmitter and receiver. Table 1.1 shows the parameters given in figure 1.1.

In a bistatic radar system, normally we indirectly measure $R_T + R_R$. We do actually measure the time difference $\tau = \tau_1 - \tau_2 = \frac{R_T + R_R - L}{c}$, but since we know L and c, we can calculate the sum $R_T + R_R$.

From geometry, the locus of all points such that the sum of the distance to two fixed points is constant, is defined as an ellipse. The two fixed points here are the transmitter and receiver, the locus of points are possible target positions. The sum of the distance is $R_T + R_R$. In

other words, when $R_T + R_R$ is measured in a bistatic radar, all possible target positions are located on an ellipsoid with focal points in the transmitter and receiver. A plot of iso-range ellipses with different values of $R_T + R_R$ is given in figure 1.2. In the monostatic case, $R_T = R_R$ and $L = 0$ and we get spheres instead of ellipsoids.
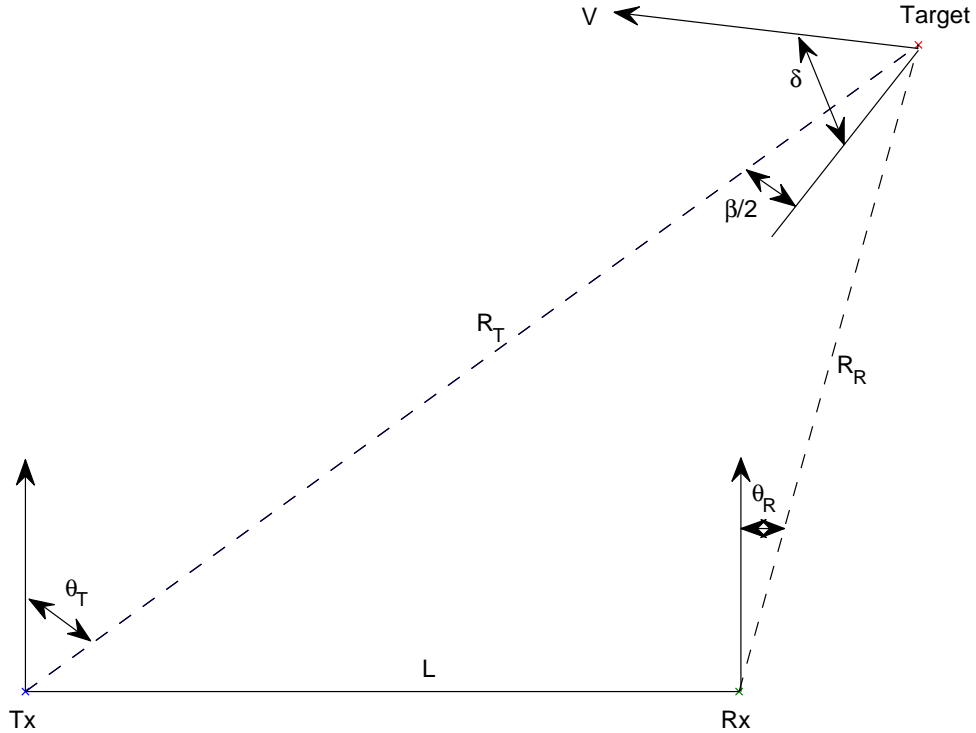

Figure 1.1: Bistatic geometry. The parameters is given in table 1.1

β	bistatic angle
θ_R	receiver looking angle
θ_T	transmitter looking angle
L	baseline
R_R	target - receiver range
R_T	target - transmitter range
V	Velocity of target
δ	Angle of velocity of target

Table 1.1: Bistatic parameters

1.2 Bistatic Radar Equation

The (S/N) (Signal to Noise ratio) for a bistatic radar is [7]

$$(S/N) = \frac{P_T G_T G_R \lambda^2 \sigma_B F_T^2 F_R^2}{(4\pi)^3 k T_s B_n L_T L_R R_T^2 R_R^2} \tag{1.1}$$

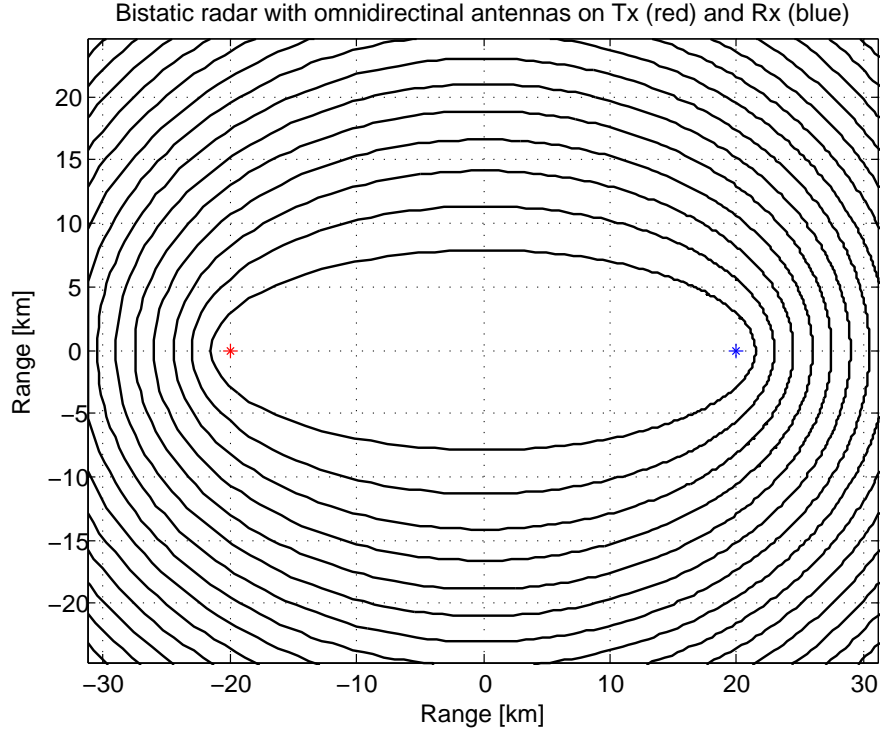Bistatic radar with omnidirectinal antennas on Tx (red) and Rx (blue)

Figure 1.2: Iso range-sum contours. Each contour is a plot of the equation $R_T + R_R = constant$

The parameters of this equation are given in table 1.2. (1.1) gives us (S/N) of a signal echoing off a target. To increase the (S/N), a solution is to integrate over time. The argumentation from ([8], p127) is to substitute B_n from (1.1) with the inverse of the coherent processing interval defined as T_I. This gives us the following equation

$$(S/N) = \frac{P_T T_I G_T G_R \lambda^2 \sigma_B F_T^2 F_R^2}{(4\pi)^3 k T_s L_T L_R R_T^2 R_R^2} \tag{1.2}$$

When integrating over an interval larger than the inverse of the bandwidth of the radar signal, we get an increase in the (S/N). For each doubling of the integration time, an increase of the (S/N) by approximately $3dB$ is expected. This type of integration is called coherent integration.

When every parameter in (1.1) except for R_T and R_R is kept constant, the contours for (S/N) are plotted, we get what is called "Ovals of Cassini". Figure 1.3 illustrates the "Ovals of Cassini" for a typical set of radar parameters. The amplitude of the contours is given in dB.

Since the constant range sum ellipses are of different shape than the constant (S/N) "Ovals of Cassini", we get different (S/N) for almost every point on the constant range sum ellipses. From figure 1.3, we see that the highest (S/N) is close to the transmitter and receiver.

R_T	transmitter-to-target range
R_T	receiver-to-target range
P_T	transmitter power output
G_T	transmitting antenna power gain
G_R	receiving antenna power gain
λ	wavelength
σ_B	bistatic radar target cross section
F_T	pattern propagation factor for transmitter-to-target path
F_R	pattern propagation factor for receiver-to-target path
k	Boltzmann's constant
T_s	receiving system noise temperature
B_n	noise bandwidth of receiver's prediction filter
T_I	coherent integration time
L_T	transmitting system losses (> 1) not included in other parameters
L_R	receiving system losses (> 1) not included in other parameters

Table 1.2: Bistatic radar equation parameters

1.3 Bistatic Range Resolution

The range resolution of all radar systems is given by the bandwidth of the radar signal. The range cell of a monostatic radar is given by the range difference of two circles with radial difference of the range resolution. This means that the range resolution is not dependent on the range from the radar. The bistatic radar has range cells given by the difference in two ellipses with range-sum difference of the range resolution, so the range resolution becomes dependent on the looking angle and bistatic range. An approximation to the bistatic range resolution is [7]

$$\Delta R_B \approx \frac{\Delta R_M}{cos(\frac{\beta}{2})} \tag{1.3}$$

where ΔR_M is

$$\Delta R_M = \frac{c}{2B} \tag{1.4}$$

where B is the bandwidth of the radar signal. ΔR_M is the corresponding monostatic range resolution.

An exact solution is given in [7], appendix B, but this is an implicit solution. This solution can be solved numerically for given bistatic parameters. The approximation is valid for β close to zero, i.e. close to the extended baseline. The approximation error becomes larger as β increases, until it falls apart when the resolution becomes infinite at $\beta = 180°$.

Figure 1.4 illustrates the range resolution for a specific configuration of the receiver antenna. The neighboring ellipses are separated by the range resolution, and the straight lines
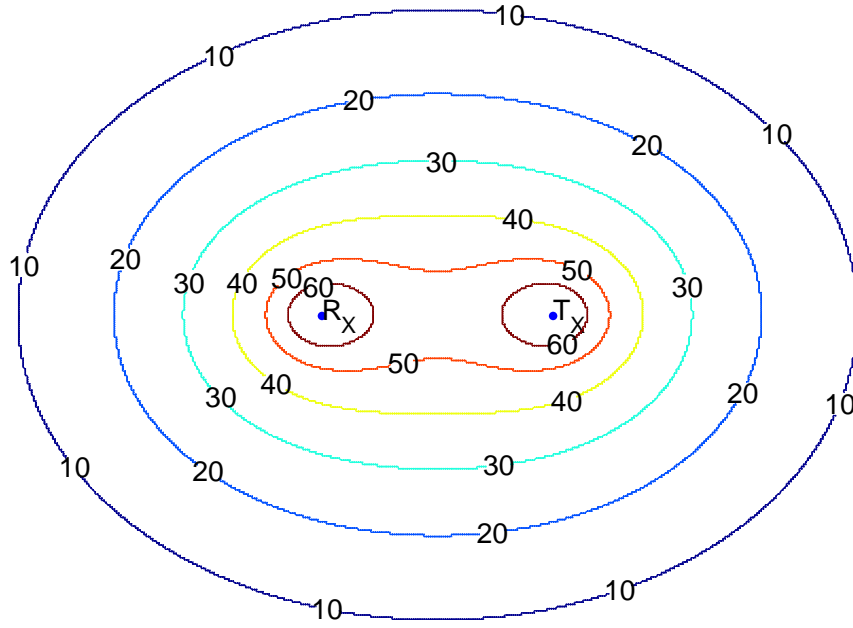
Figure 1.3: Contours of the bistatic radar equation. The amplitude is given in dB. Each contour shows a constant (S/N), and they are called "Ovals of Cassini". The amplitude is largest close to the transmitter and receiver.

intersecting each of the ellipses denotes the receiver antenna direction. The figure shows the dependency on range and β for the range resolution.

1.4 Bistatic Doppler

The Doppler shift of a reflected signal, ignoring the relativistic effects, is given by

$$f_B = \frac{1}{\lambda}\left[\frac{d}{dt}(R_T + R_R)\right] \tag{1.5}$$

where λ is the wavelength of the signal. The quantities $\frac{dR_R}{dt}$ and $\frac{dR_T}{dt}$ can be found by projecting the target velocity vector onto R_R and R_T. This gives us the following equation

$$f_B = \left(\frac{2V}{\lambda}\right)cos(\delta)cos(\beta/2) \tag{1.6}$$

where V and δ can be found in table 1.1. Figure 1.5 displays the Doppler shift as a function of the direction of the velocity vector, angle δ for different bistatic angles. $\beta = 0°$ gives Doppler shift in the monostatic case, and $\beta = 180°$ gives zero Doppler shift for all δ.

If we define the bistatic velocity v_B as follows

$$v_B = \frac{1}{2}\frac{d}{dt}(R_T + R_R) = V cos(\delta)cos(\beta/2) \tag{1.7}$$

we can rewrite (1.5) to

$$f_B = \frac{2v_B}{\lambda} \tag{1.8}$$

Bistatic radar with omnidirectinal antennas on Tx (red) and directional antenna on Rx (blue)
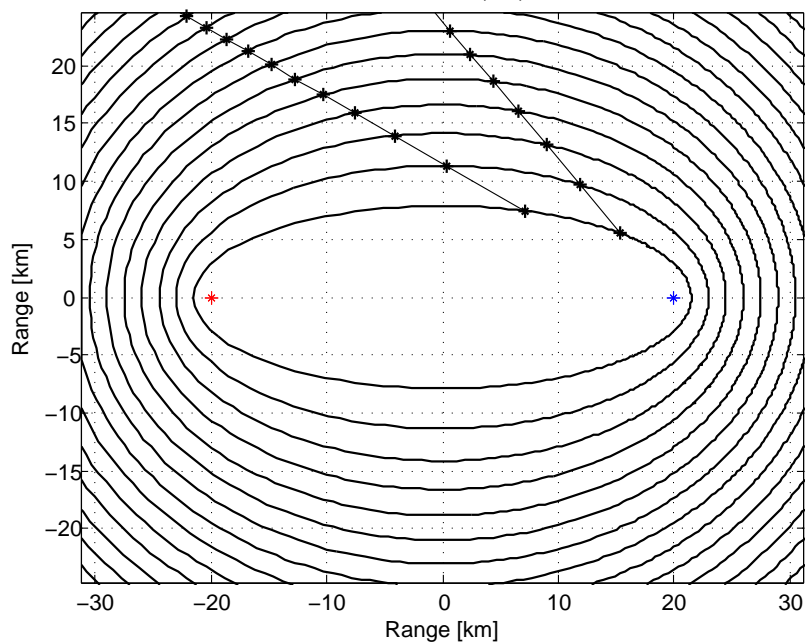

Figure 1.4: Plot displaying the range resolution in a direction with directional receiver antenna. The bistatic range resolution is different for different range sums and β.

We see that the Doppler shift is dependent on the wavelength of the signal, and the Doppler shift is therefore frequency dependent.

The Doppler resolution of a radar system is dependent on the integration time in the following way

$$\Delta f = \frac{1}{T_I} \tag{1.9}$$

where Δf is the Doppler resolution and T_I is the integration time.
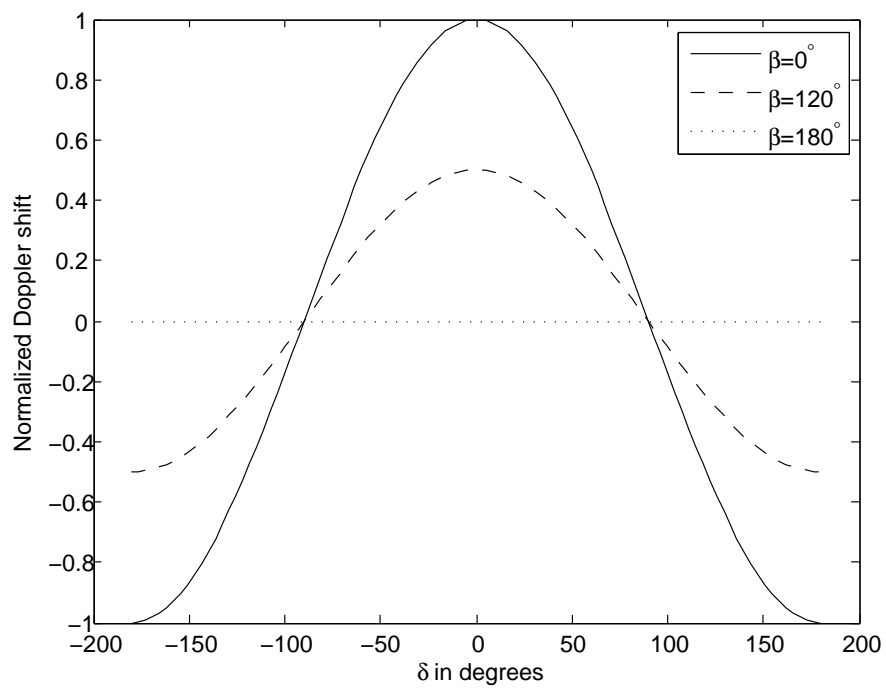
Figure 1.5: Doppler shift as a function of the velocity vector, angle δ for different bistatic angles [7]. $\beta = 0°$ give monostatic Doppler shift.

2 Digital Video Broadcast - Terrestrial

DVB-T is the digital television broadcast system used in Norway and many other countries. It is based on a digital modulation of the signals. This section will present the DVB-T signal form and properties. It will also present the DVB-T transmitter network structure, and all other information relevant to DVB-T as a PBR illuminator.

2.1 DVB-T signal

The DVB-T signal has the form [2]

$$s(t) = Re\left\{e^{j2\pi f_c t}\sum_{m=0}^{\infty}\sum_{l=0}^{67}\sum_{k=K_{min}}^{K_{max}}c_{m,l,k}\times\psi_{m,l,k}(y)\right\} \tag{2.1}$$

$$\psi_{m,l,k}(t) = \begin{cases} e^{j2\pi\frac{k'}{T_U}(t-\Delta-l\times T_s-68\times m\times T_s)} & (l+68\times m)\times T_s \leq t \leq (l+68\times m+1)\times T_s \\ 0 & else \end{cases}$$

Where the parameters are:

k	carrier number
l	OFDM(Orthogonal Frequency Division Multiplexing) symbol number
m	transmission frame number
K	number of transmitted carriers
T_S	symbol duration
T_U	inverse of the carrier spacing
Δ	guard interval
f_c	central frequency of RF signal
k'	carrier index relative to center frequency, $k' = k - \frac{K_{max}-K_{min}}{2}$
$c_{m,l,k}$	complex symbol for carrier k of the data symbol no. l in frame number m

Table 2.1: DVB-T signal parameters [2]

Looking at one frame in sampled, down modulated and complex form gives us the equation

$$s(n) = \sum_{k=-K/2+1}^{K/2} c_{k+K/2}\times e^{j2\pi\frac{n}{N_u}k} \tag{2.2}$$

Where $N_u = f_s T_U$. This equation is recognized as a $IDFT$ (Inverse Discrete Fourier Transform) of c_k when $f_s = K/T_U$. Almost all DVB-T modulators/demodulators use the $IFFT/FFT$ (Inverse Fast Fourier Transform/Fast Fourier Transform) for increased speed.

This signal form is called Orthogonal Frequency Division Multiplexing. The name comes from the orthogonality of the sinusoids summed together. The spectrum of the signal almost has the form of a rectangular window(it is really a sum of frequency spaced *sinc* functions).

The modulation of the complex symbols $c_{m,l,k}$ is either QPSK (Quadrature Phase Shift Keying), 16-QAM (Quadrature Amplitude Modulation) or 64-QAM. The modulation defines where in the complex plane the symbols are placed. The Norwegian DVB-T system has the following parameters

Number of carriers	$K = K_{max} - K_{min}$	6817
Symbol duration	T_U	$896\mu s$
Carrier spacing	$\frac{1}{T_U}$	$1116Hz$
Spacing between carriers K_{min} and K_{max}	$\frac{K-1}{T_U}$	$7.61MHz$
Guard interval	$\frac{\Delta}{T_U}$	$\frac{1}{4}$
Duration of guard interval	Δ	$224\mu s$

Table 2.2: Table of parameters in the Norwegian DVB-T system

Figure 2.1 displays the DVB-T spectrum.

A promising characteristic of the DVB-T signal is the constant bandwidth. For FM based PCL systems, a potential problem is the bandwidth of the signal which is dependent on the audio transmitted. If the radio program goes silent, the bandwidth drops almost to zero. Since the DVB-T signal is OFDM, the bandwidth will never disappear. A waterfall plot of the DVB-T signal over the course of 24 hours is given in figure 2.2.

DVB-T uses the standard UHF television channels to denote the center frequency. The UHF channels and their corresponding frequencies are listed in table 2.3.

2.2 DVB-T signal properties

The spectrum of the DVB-T signal is, as mentioned in the last subsection, a sum of equally spaced *sinc* functions. The modulation of the complex symbols is such that they never have zero amplitude. And the properties of the DVB-T interleaver and the MPEG(Moving Picture Experts Group) codec give us an almost random signal. This means that the spectral density will resemble a band limited white noise process, which has a spectral density form of a rectangular window. The randomness of the DVB-T signal is analyzed in [1].

Since the DVB-T signal is a noise like signal, the autocorrelation function of the signal will have the shape of a thumbtack. There are some deterministic components inserted into the signal for the demodulator to be able to synchronize to the signal frames. These deterministic components are the guard interval and the pilot tones.

The guard interval is the insertion of a copy of the last bit of the frame before the beginning
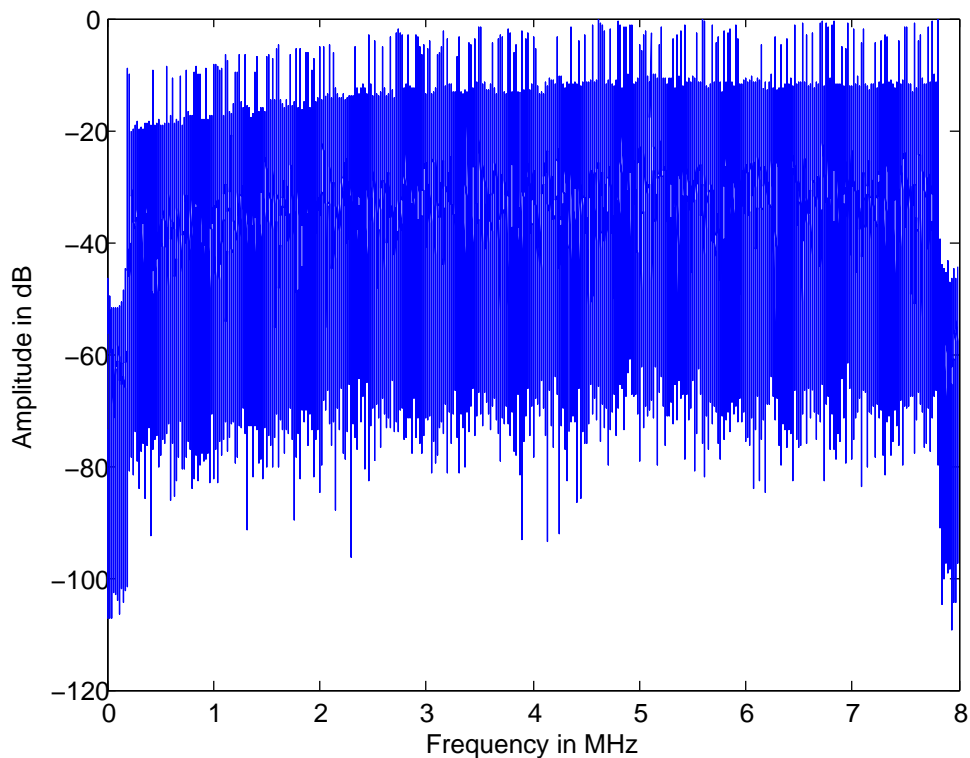
Figure 2.1: The DVB-T spectrum. The continual pilots are clearly of larger amplitude than rest of signal due to long integration time.

of the frame. The pilot tones are carriers at given positions with a deterministic amplitude and phase.

This produces some non-zero ambiguities in the autocorrelation, both in Doppler and delay. Figure 2.3 shows the autocorrelation function of a DVB-T signal. We see that there are several ambiguities other than in zero range and zero Doppler. The ambiguities are expected because of the insertion of deterministic components in the DVB-T signal.

Since the DVB-T signal is digital, it is possible to decode the signal. This is positive for a PBR system because it makes it possible to recreate a noise free reference channel.

Since the ambiguities are stationary, the tracker will treat them as clutter and they will not pose a problem for the radar system.

2.3 DVB-T transmitter network

The DVB-T transmitters are configured as a number of Single Frequency subnetworks. This is possible due to the guard interval used in the DVB-T signal. Maximum distance between the transmitters in the same SFN is given as $\Delta \times c$, where Δ is defined in table 2.1 and c is the speed of light. For a PBR system, this could give several targets in the processing, due

UHF Channel	Center frequency		UHF Channel	Center frequency
21	474 MHz		45	666 MHz
22	482 MHz		46	674 MHz
23	490 MHz		47	682 MHz
24	498 MHz		48	690 MHz
25	506 MHz		49	698 MHz
26	514 MHz		50	706 MHz
27	522 MHz		51	714 MHz
28	530 MHz		52	722 MHz
29	538 MHz		53	730 MHz
30	546 MHz		54	738 MHz
31	554 MHz		55	746 MHz
32	562 MHz		56	754 MHz
33	570 MHz		57	762 MHz
34	578 MHz		58	770 MHz
35	586 MHz		59	778 MHz
36	594 MHz		60	786 MHz
37	602 MHz		61	794 MHz
38	610 MHz		62	802 MHz
39	618 MHz		63	810 MHz
40	626 MHz		64	818 MHz
41	634 MHz		65	826 MHz
42	642 MHz		66	834 MHz
43	650 MHz		67	842 MHz
44	658 MHz		68	850 MHz

Table 2.3: The UHF Television channels and their center frequencies

to one target in the air. More complex processing is therefore needed to remove the false targets.

A map displaying the Norwegian transmitter network as a function of it's transmitter power is given in figure 2.5. The transmitters are placed such that the coverage is planned to be approximately 95% of the households in Norway. This does not mean that the coverage is 95% of the area of Norway. The population is sparse in some areas, so full area coverage is not expected.
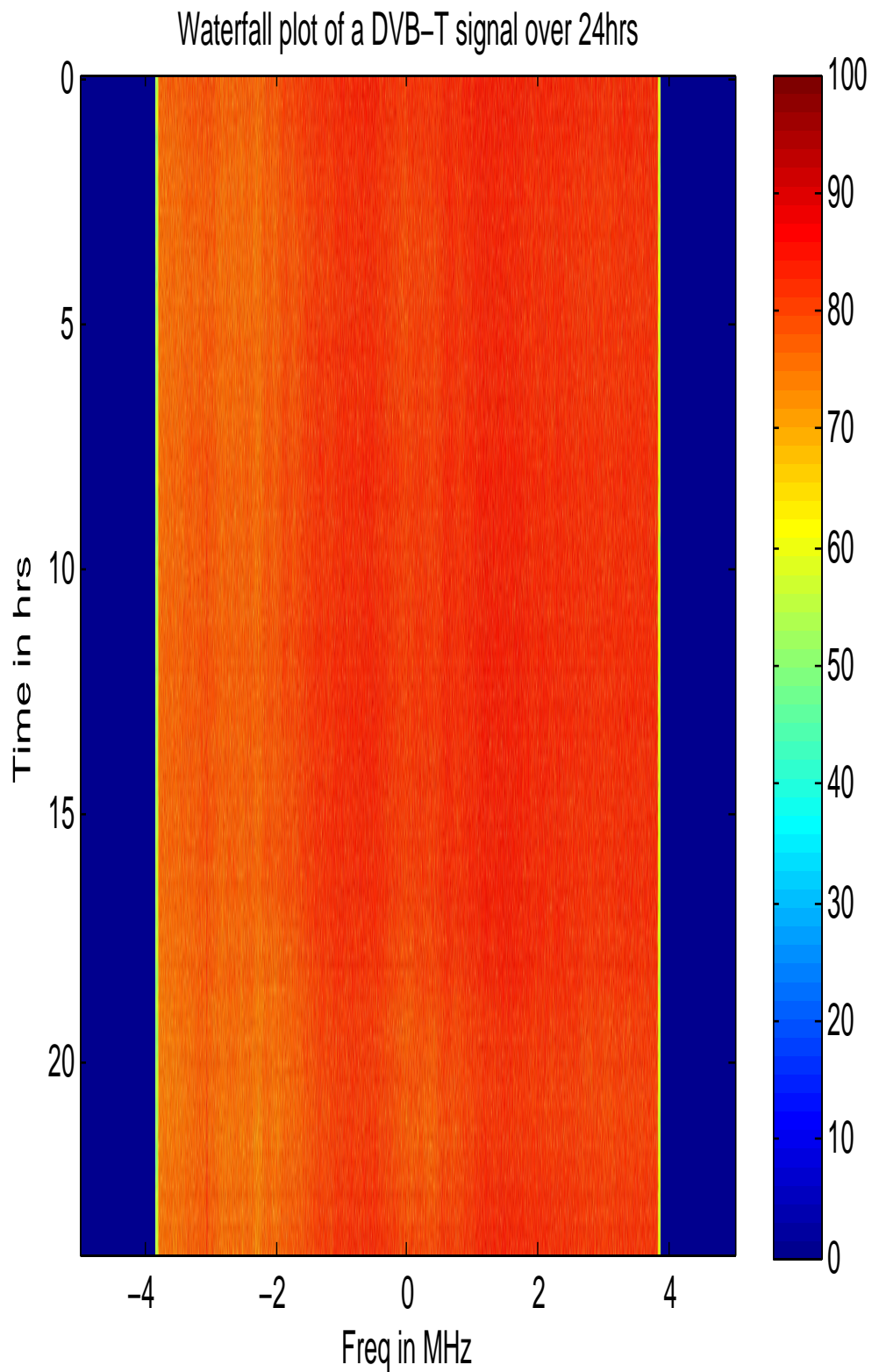
Figure 2.2: Waterfall plot of the DVB-T signal taken over the course of 24 hours. The bandwidth is stable over time.
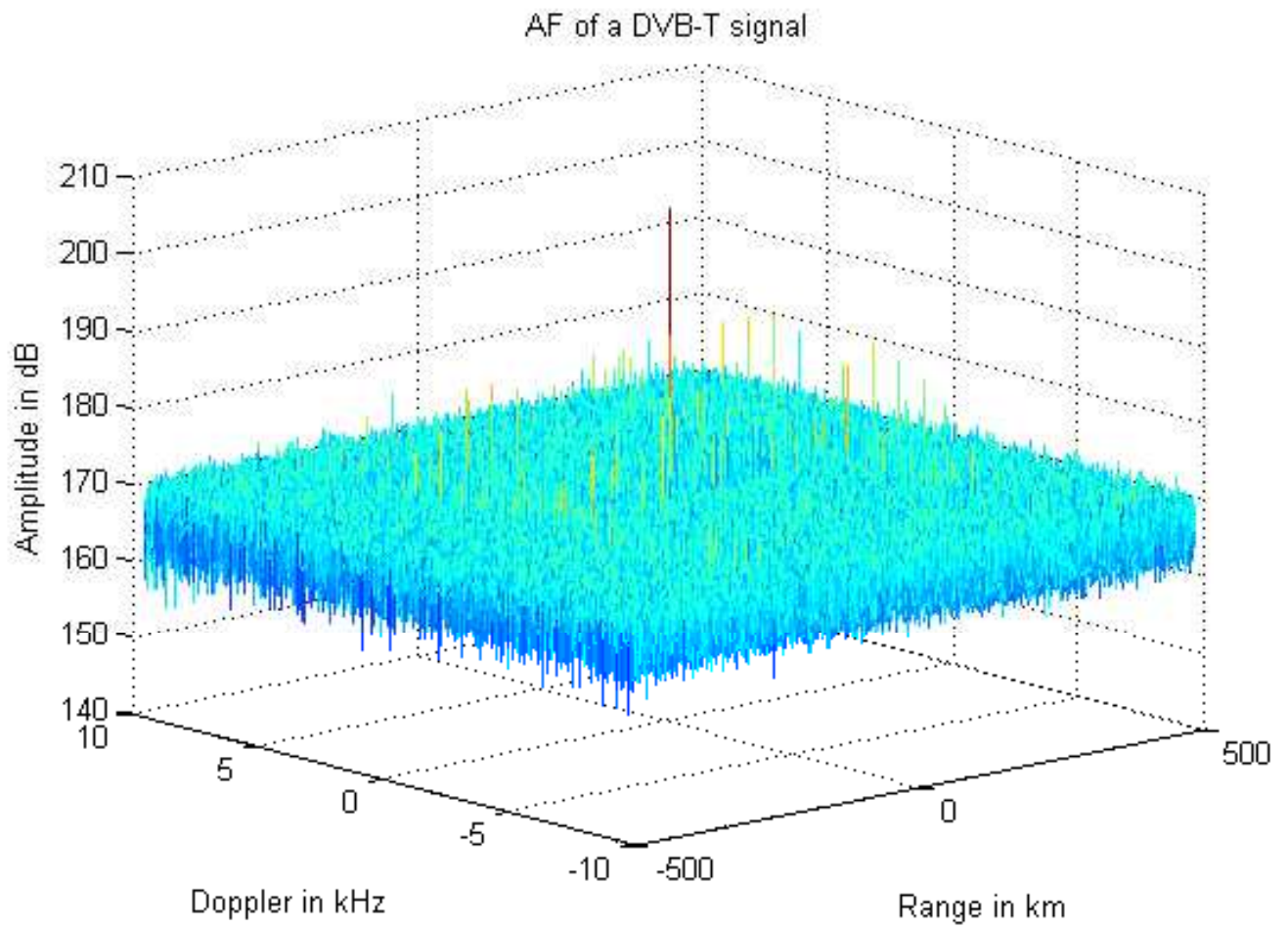
Figure 2.3: The AF of a DVB-T signal. The ambiguities from guard interval and pilot tones stands out over the noise floor for non-zero range and Doppler.
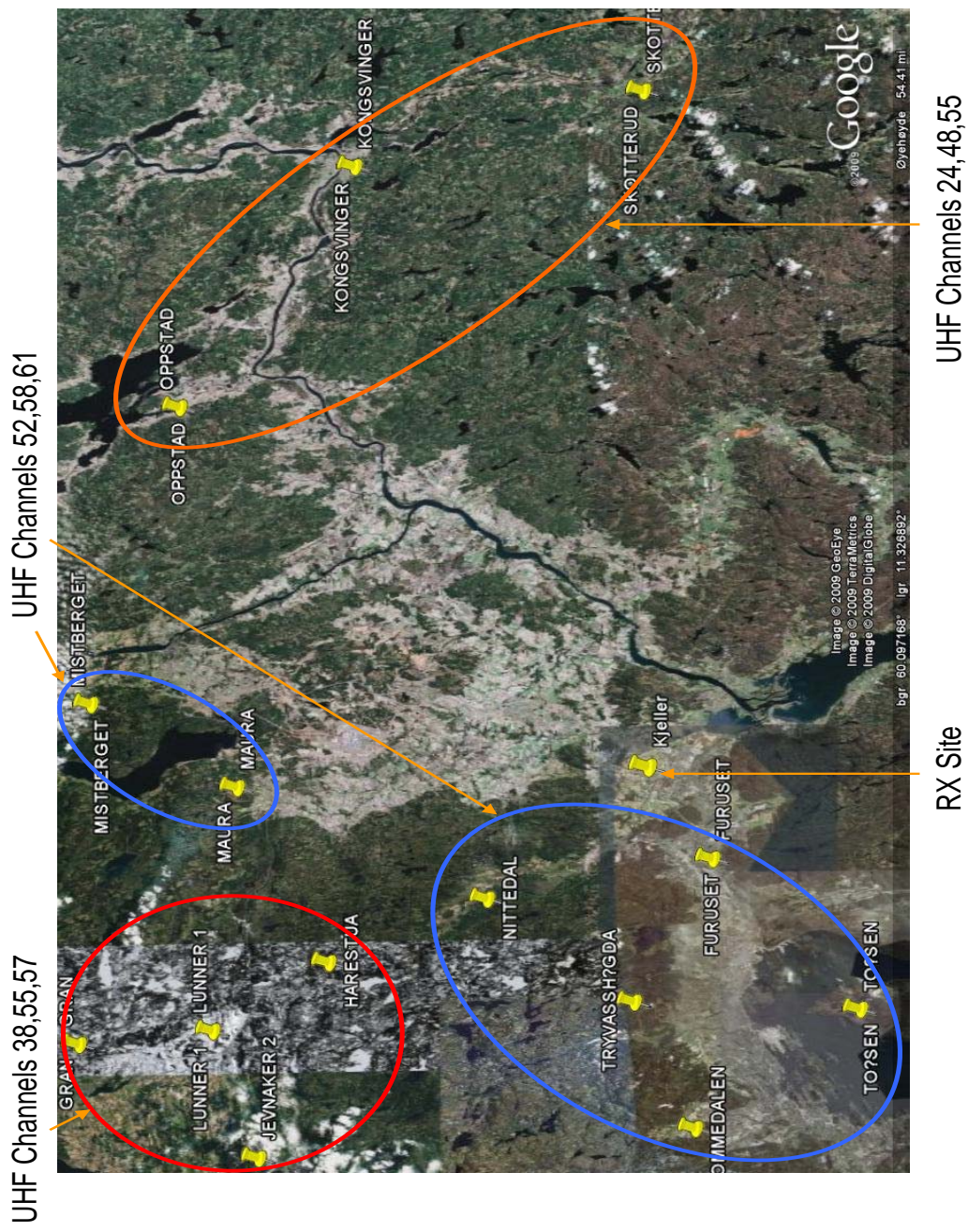
Figure 2.4: Displaying DVB-T transmitter network in Akershus, Norway. The different single frequency subnetworks are circled.
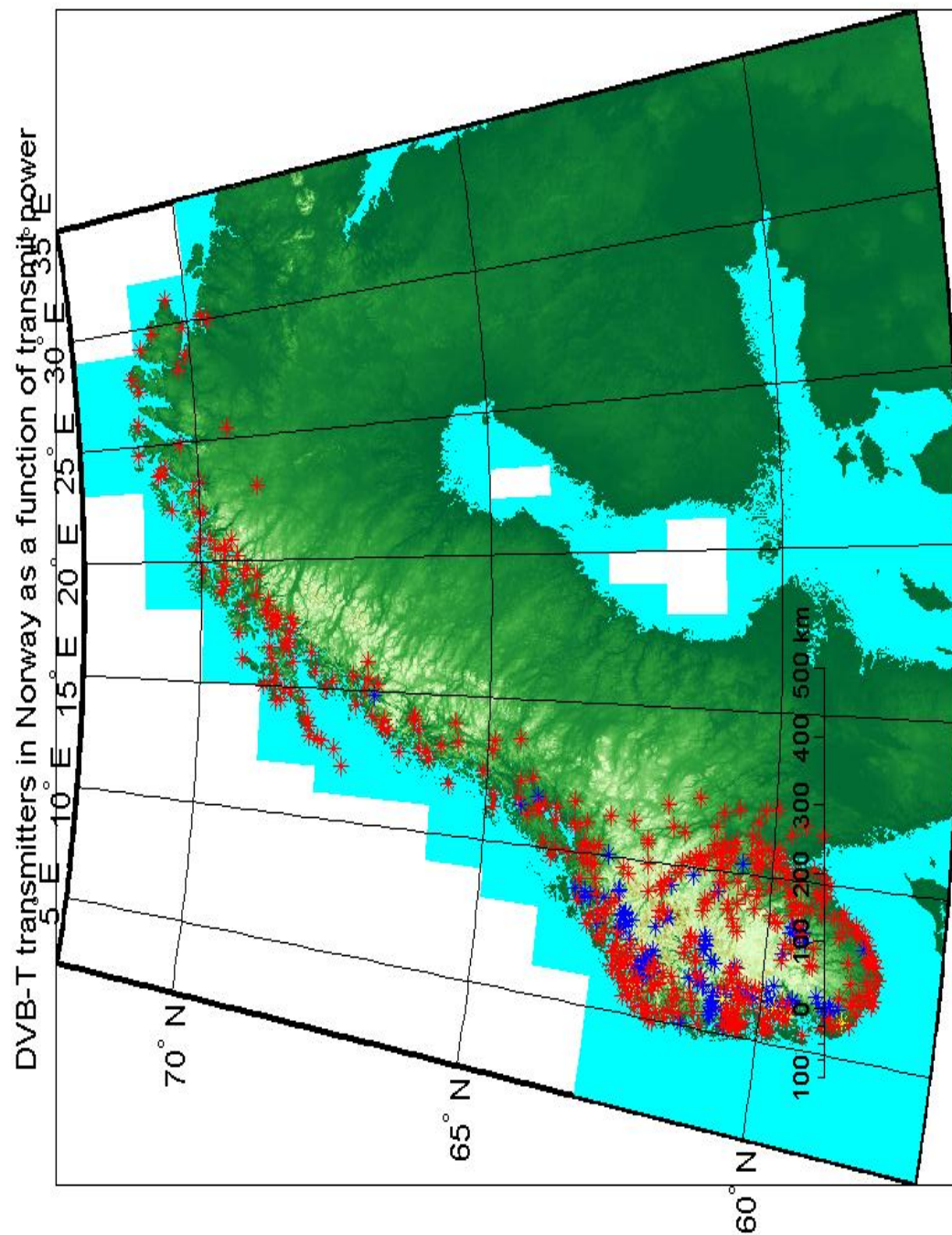
Figure 2.5: Displaying DVB-T transmitters in Norway as a function of transmitter power. The DVB-T coverage of Norway will be approximately 95% of the households.

3 The PBR sensor hardware

The PBR sensor consists of two pieces of equipment:

1.) The antennas, which are standard digital TV antennas fixed at the roof of FFI (Forsvarets forskningsinstitutt). They are equipped with cameras and servo motors, to be able to follow targets over the sky. Figure 3.4 shows how the antennas are set up. The reference antenna is a narrow lobe antenna with high gain, and the surveillance antenna has a wide lobe and high gain. The surveillance antenna has an amplifier to give the required gain for surveillance operation.

2.) The other part of the sensor is the recording equipment. The recording equipment is fixed in a rack, and consists of three computers. One computer is the control PC, which controls the recording process and controls other hardware such as the ADS-B (Automatic dependent surveillance-broadcast) recorder and the DQD2 (Dual Quadratic Demodulator 2). The other two computers are dedicated recording PC's, recording one channel each. Figure 3.1 shows the rack and the different hardware.

3.1 Control PC

The control PC controls the different pieces of hardware used in the sensor. The computers are connected through a gigabit LAN (Local Area Network) to ensure high enough bandwidth for data exchange and control signals.

The control software for the recording PCs is developed by SAGAX, the manufacturers of the ADC (Analog to Digital Converter) in the recording PCs. Also, the control PC control the ADS-B data retriever hardware and the DQD2 down modulator.

3.2 Recording PC's

Each recording PC is equipped with an ADC with a bandwidth of 40MHz. The ADCs and control PCs are built by a Hungarian company called SAGAX. They were designed after specs from FFI. The ADC's are synchronized, so the recordings on each channel can be synchronized.

The storage in the recording PCs is of 3TB in size and makes it possible for approximately 5 hours of continuous radar recording. The storage is setup as a RAID system to increase the writing speed to the required 160MB/s. The required 160MB/s is because of the bandwidth and resolution of the ADCs.

Recording PC 1 is connected to the reference antenna through the DQD2, and is usually pointed towards a DVB-T transmitter of choice. Recording PC 2 is connected to the surveillance antenna through the DQD2, and is usually pointed towards a target.

3.3 DQD2

The DQD2 is a dual quadratic down modulator, designed at FFI. It can filter and down modulate four different UHF channels of $8MHz$ bandwidth each. It places each channel in one of the intervals $(1 - 9MHz), (11 - 19MHz), (21 - 29MHz), (31 - 39MHz)$, has two antenna inputs. Input of the DQD2 is the two antennas and a control input. Output is two signals at baseband with a bandwidth of $40MHz$. These outputs are connected to the ADC's of the recording computers. Figure 3.3 shows a schematic of the DQD2, and figure 3.2 shows how the DQD2 functions.

The control software is written at FFI, and the DQD2 is controlled through a USB (Universal Serial Bus) interface.

3.4 ADS-B

ADS-B is a cooperative surveillance technique used by air traffic control. ADS-B equipped airplanes send out state and other type of information. The state information is position, velocity and time. This gives us the possibility of calculating a good reference position and velocity in the bistatic plane, if the information is reliable.

The state information is sometimes unreliable because of the use of IMU (Inertial Measurement Unit) as reference source. These devices lose accuracy over time, and the accuracy for an airplane who has been in the air for some time may be poor.

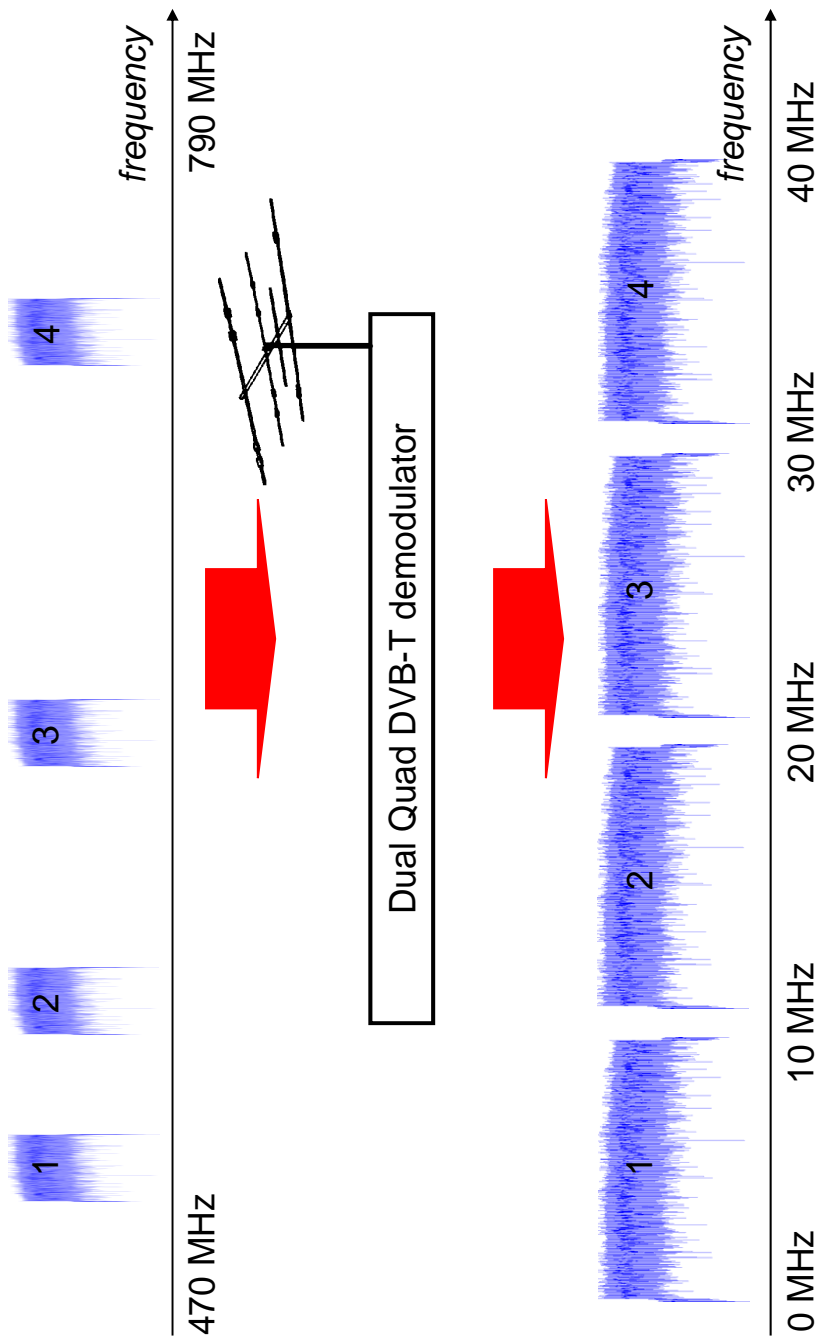*Figure 3.1:* The hardware rack with the recording PC's, control PC and other hardware such as ADS-B receiver and DQD2

Figure 3.2: Displays the function of DQD2. Down modulates four UHF channels simultaneously for two channels
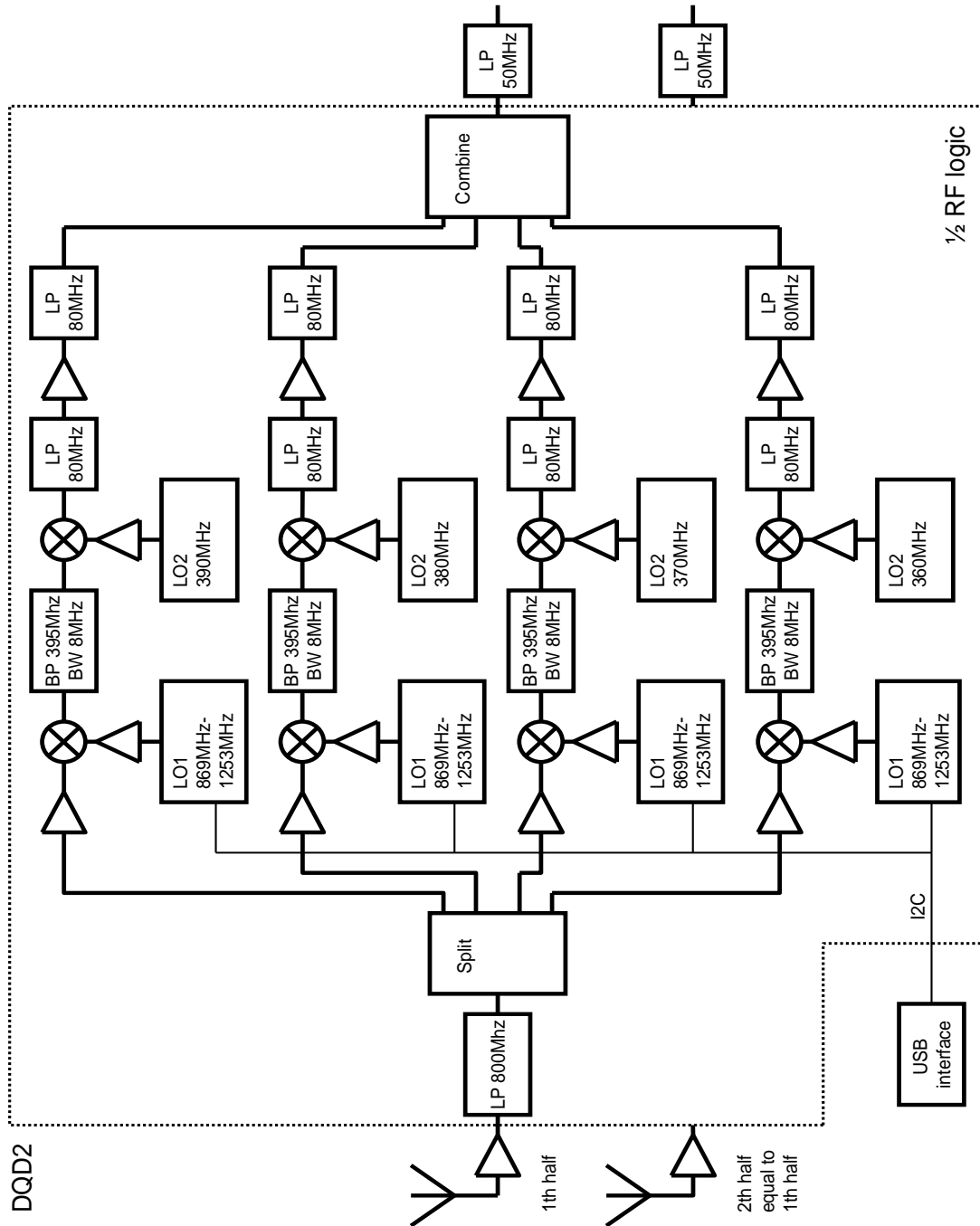
Figure 3.3: A schematics of the DQD2

(a) Reference channel, FM radio antenna; TRIAX 5 element (upper antenna), DVB-T antenna; Televes DAT75 Digital Tv Aerial (lower antenna).

(b) Surveillance channel, DVB-T antenna; Funke Digital TV FFA4522 21/69 (upper antenna), FM radio; TRIAX 5 element (lower antenna).

Figure 3.4: The reference and surveillance channel antennas, mounted on an metal rod, on top of a pan- and tilt-device with video camera for remote (lab) oparations.

4 Processing techniques

This section will present the processing technique used in this PBR system. It will also present an alternative technique.

4.1 The Ambiguity Function

The ambiguity function correlates two signals s_1 and s_2 against each other, frequency shifting one of the signals. The ambiguity function will in the following be referred to as AF (Ambiguity Function), unless otherwise stated. The AF is often used in radar processing because it gives the possibility of both range and Doppler processing. The AF is defined as [6]

$$A(\tau, f) = \int_{-\infty}^{\infty} s_1(t) s_2^*(t - \tau) e^{-j2\pi ft} dt \tag{4.1}$$

where τ is the time delay, and f is the frequency shift. The function correlates s_1 with a delayed and frequency shifted s_2.

The correlation used throughout this work is an implementation of

$$\chi(n, m) = \sum_{k=0}^{N-1} s_1(k) s_2^*(k - n) e^{-j2\pi \frac{m}{N-1} k} \quad , \quad 0 < n < N - 1, \quad 0 < m < N - 1 \tag{4.2}$$

See [4] for the implementation adapted for use in this work.

The implementation is in MATLAB, and consists only of $FFT/IFFT$'s and complex multiplications, so it is highly efficient.

4.2 Doppler-delay plots

This subsection will define what Doppler-delay plot and accumulated Doppler-delay plot is. The Doppler-delay plot is a two dimensional surface, plotting $|\chi(n, m)|$, given in (4.2). In a PBR system, this surface constitutes the correlation between the reference and surveillance signal. A peak in the correlation is one of three things. Ambiguities caused by properties of the transmitted signal, clutter from reflection of static objects or direct signal from transmitters in the single frequency subnetworks, or a target. The radar system to be operational must separate the two first points from the last. This is usually done by the tracker, but this will not be discussed in this work. A typical Doppler-delay plot containing all of these types of peaks is given in figure 4.1. Here, $|\chi| = 0dB$ is the noise floor.

A second type of plot used in this work is the accumulated Doppler-delay plot. Here, we use several consecutive Doppler-delay plots, threshold each of them with a given threshold, and *or* them together. This gives the characteristic plot give in figure 4.2.

These types of plots will be used extensively throughout this work.
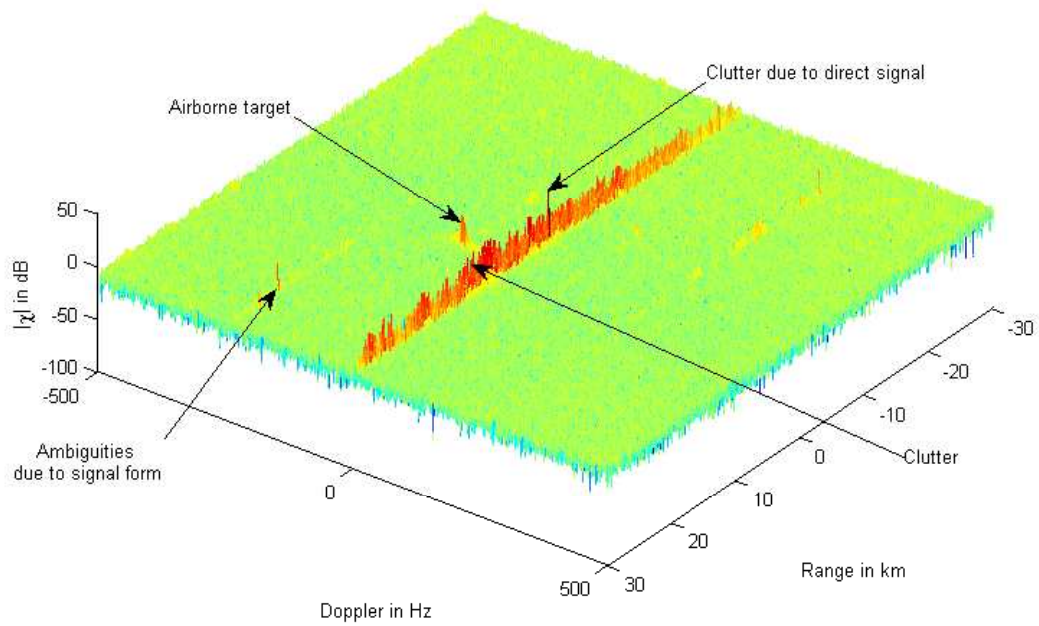
Figure 4.1: Doppler-delay plot. Shows the DSI, noise floor and ambiguities from signal coding and target.
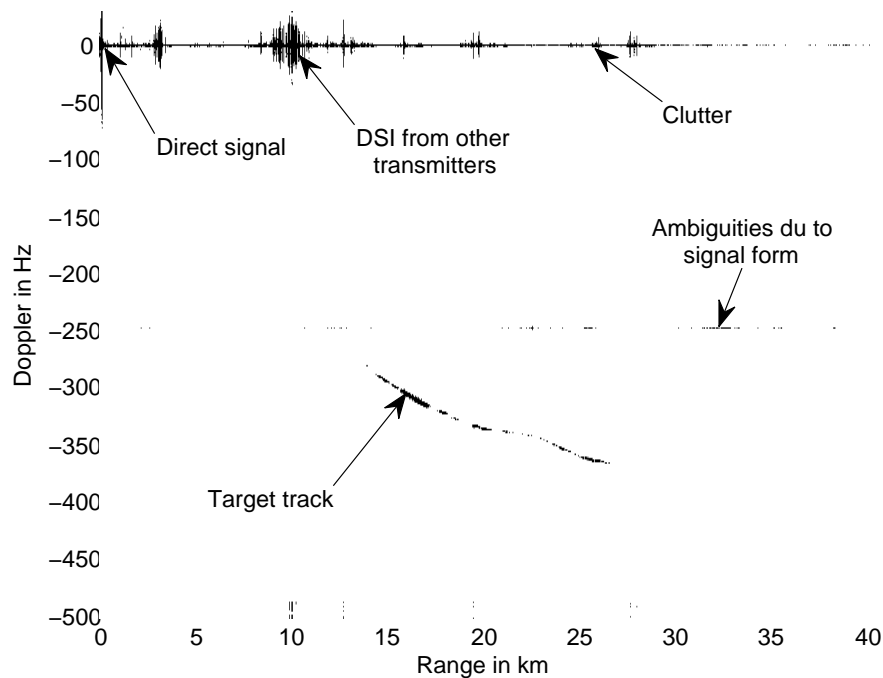

Figure 4.2: Accumulated Doppler-delay plot, produced by a real PBR dataset. Shows the DSI, clutter ambiguities from signal coding and target track.

4.3 Range walk

Range walk is a phenomenon occurring when the target moves over several range cells during the integration time. This leads to an energy dispersal in the correlation. Range walk has a low probability of occurring when the inequality

$$v_B T_I << \frac{c}{B} \tag{4.3}$$

is satisfied. Here, v_B is the bistatic velocity, T_I is the integration time and B is the bandwidth of the radar signal. If the inequality

$$\frac{c}{B} < v_B T_I \tag{4.4}$$

is satisfied, range walk will occur, and must be dealt with somehow.

Range walk can both decrease the signal to noise ratio, and decrease the range resolution of the system. These are consequences that may have an impact on the performance of the radar system.

This is illustrated in figure 4.3, where we see cross section in range of a target in two positions. It is a real data set with a real target, and the effects of range walk are illustrated. Increasing the integration time widens the main-lobe and the (S/N) does not increase with the expected ratio.

Figure 4.4 shows the geometry of the target in the four plots in figure 4.5, (a), (b), (c) and (d). The target has a constant angle of velocity ϕ, and a constant velocity. These constants are given in a Cartesian coordinate system, and the target has no acceleration in this reference frame. The bistatic velocity is dependent on both δ and β (1.8), and range walk may therefore not happen in some regions of the bistatic plane. This is because the bistatic velocity may for some positions yield zero.

The four plots in figure 4.5 display a normalized bistatic velocity as a function of coordinates, given constant velocity and direction as mentioned above. Black means zero bistatic velocity, and white means maximum absolute bistatic velocity. Figure 4.5, (a) shows the geometry for $\phi = 0°$, (b) for $\phi = 30°$, (c) for $\phi = 60°$ and (d) for $\phi = 90°$. Since range walk is dependent on the bistatic velocity, the figures display where there is risk of range walk for some target directions. White means high risk of range walk, given large enough bistatic velocity compared to coherent integration time, and black means low risk of range walk.
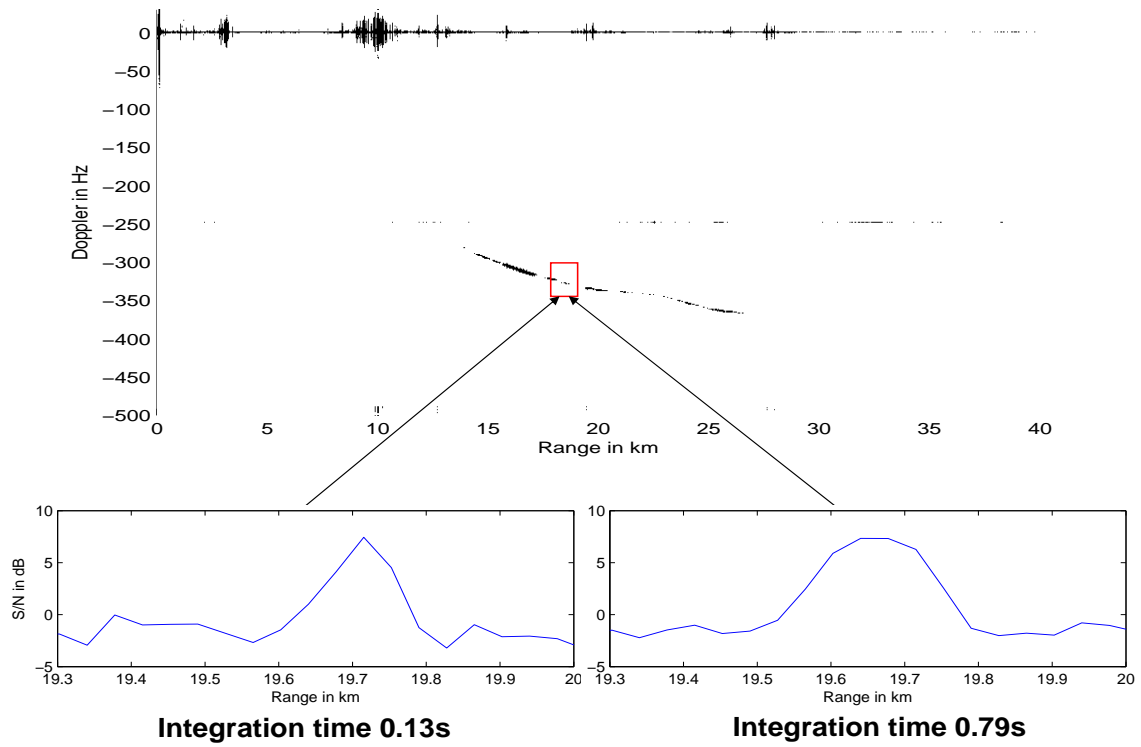
Figure 4.3: Range walk of a target, produced by real PBR dataset. This shows energy dispersal in the range direction.
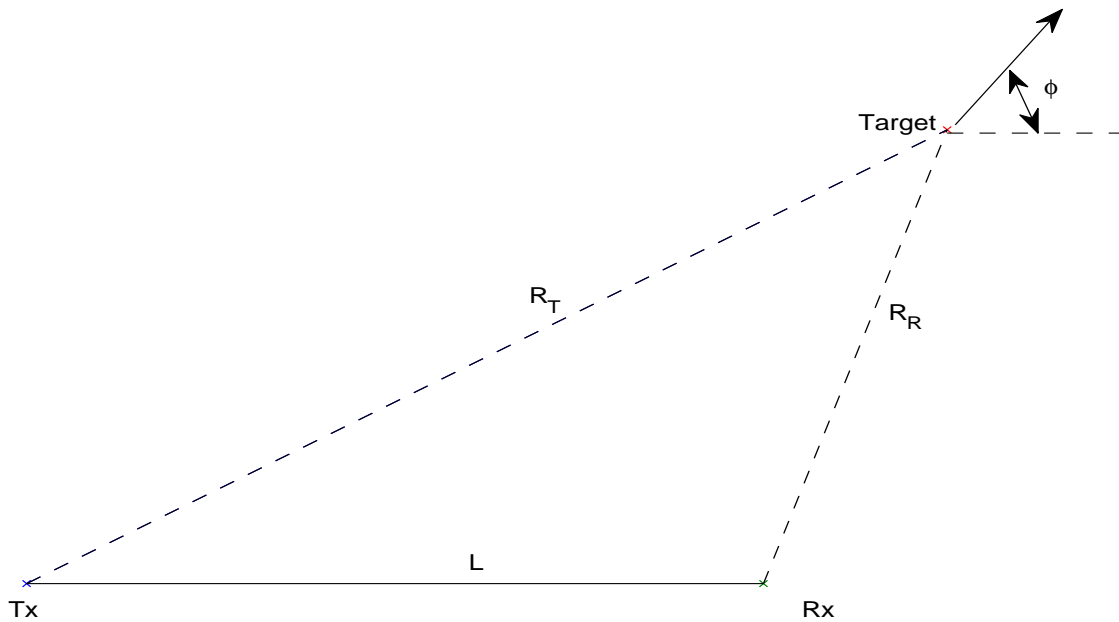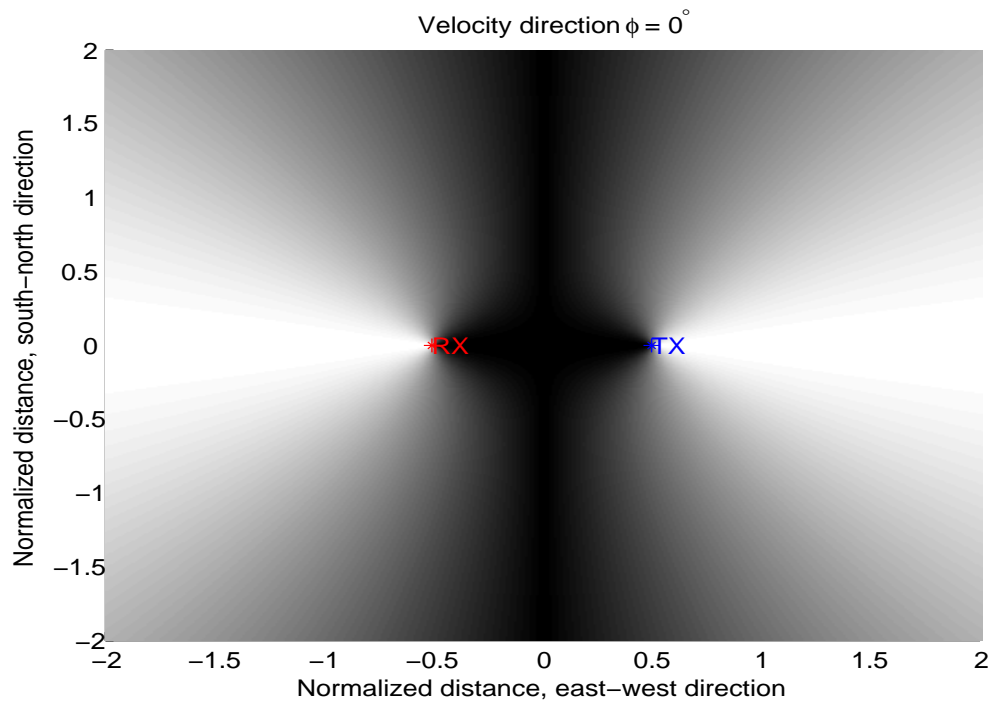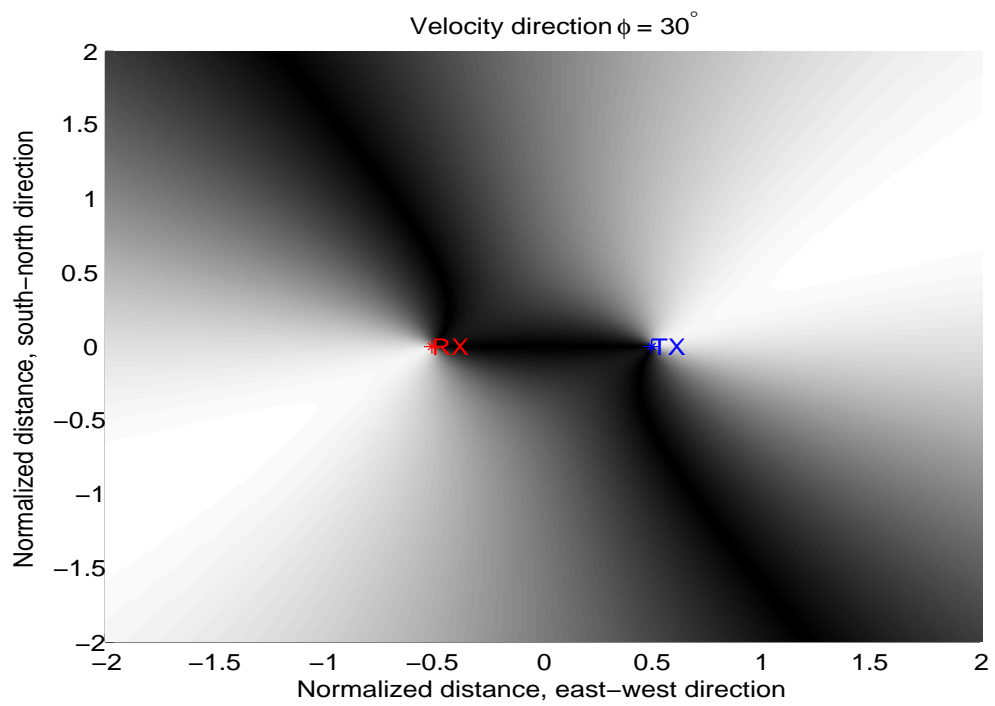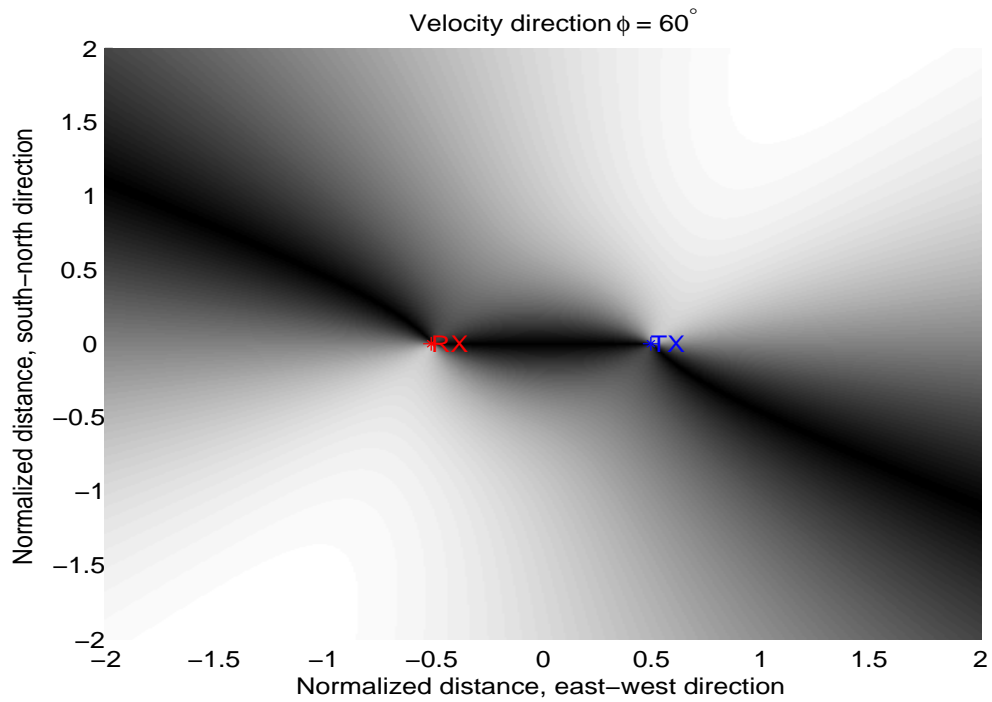

Figure 4.4: Geometry of the figures describing range walk in the bistatic plane. The angle ϕ denotes the direction of velocity of the target.
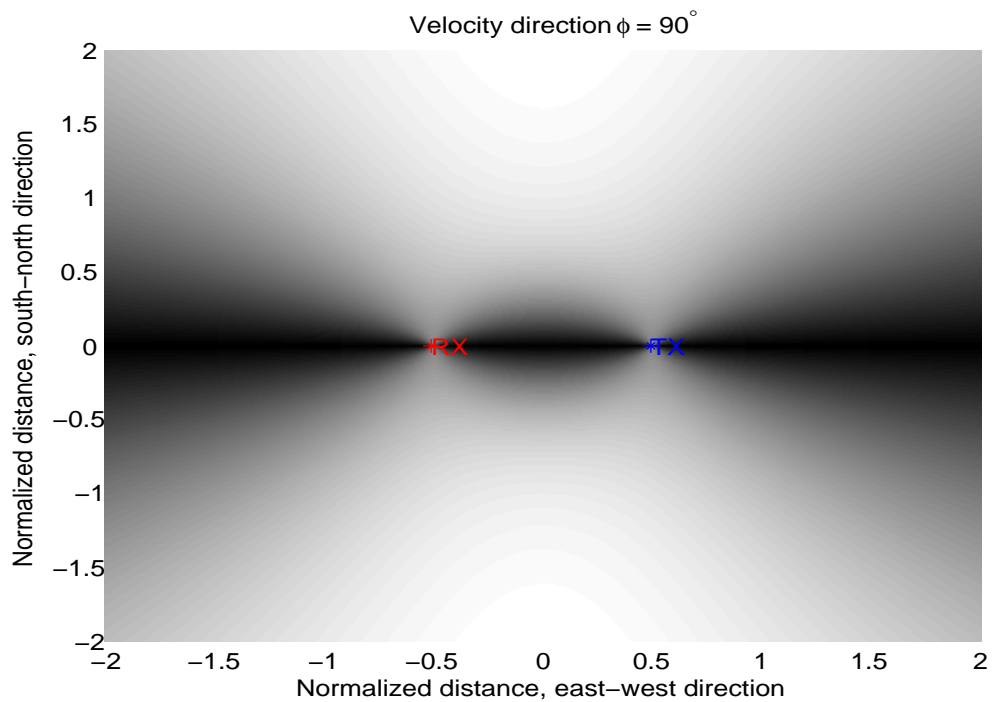
(a) Target angle of 0°

(b) Target angle of 30°

(c) Target angle of 60°

(d) Target angle of 90°

Figure 4.5: This figure denotes the bistatic velocity of a target, given constant rectilinear velocity and direction in a Cartesian coordinate system. In other words, the target has a straight path with a constant velocity.

4.4 Doppler walk

Doppler walk is a phenomenon occurring when the target moves over several Doppler cells during the integration time. As with range walk, it will lead to energy dispersal in the correlation. Doppler walk has a low probability of occurring when the inequality

$$T_I^2 a_B << \frac{\lambda}{2} \tag{4.5}$$

is satisfied. Here, a_B is the bistatic acceleration, T_I is the integration time and λ is the wavelength of the radar signal. If the inequality

$$\frac{\lambda}{2} < T_I^2 a_B \tag{4.6}$$

is satisfied, Doppler walk will occur, and must be dealt with somehow.

As with range walk, Doppler walk can decrease (S/N) and widen the target response in Doppler.

This is illustrated in figure 4.6, where we see a cross section in Doppler of a target for two different positions. The data is a real dataset of a target, and the effects of Doppler walk are illustrated. The main-lobe is widening, and the (S/N) is not increased with the expected ratio.
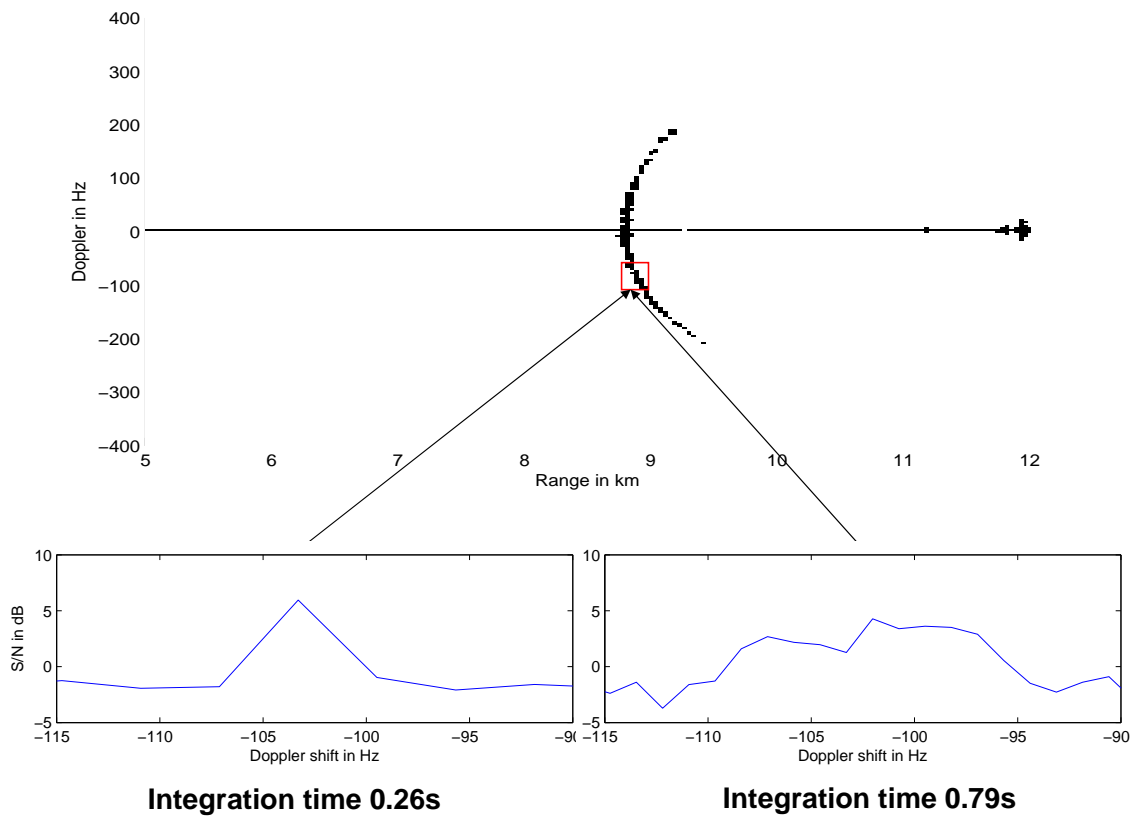
Figure 4.6: Doppler walk of a target, produced by a real PBR dataset. This shows energy dispersal in the Doppler direction.

4.5 Power Density

The following equation ([8], equation 6.1) displays the power density at a point R away from the transmitter, given a pattern propagation factor F_T. The power density illustrates the signal energy loss due to propagation.

$$\Phi = \frac{P_T G_T}{4\pi R^2} F_T^2 \qquad (4.7)$$

5 Simulations

This section will simulate a DVB-T based PBR system with the processing techniques used later in the real system.

5.1 The simulator

The simulator consists of an DVB-T signal generator, target simulator and a radar processor. Figure 5.1 shows a block diagram representation of the DVB-T based PBR system simulator. It consists of three different parts. The DVB-T signal generator, target generator and the radar processor. For explanation of the different blocks, section 2 defines the DVB-T signal, section 4 defines the processing technique and the targets are given by a RCS(Radar Cross Section) and propagation loss equal to A_p, time delay proportional to the range sum of $r_p(n)$ and Doppler shift of $f_p(n)$, where $p\epsilon[1,...,P]$ for P simulated targets.

The data stream used in the DVB-T signal generator is generated by a random process. The modulation symbols $c_{m,k}$ are uniformly distributed in the positions defined by a 64-QAM modulation. All the complex symbols $c_{(m,k)}$ are randomly generated except for the pilot tones. This is a good approximation of a real DVB-T signal because the MPEG coder and interleaver randomize the signal, so it is close to a band limited, white Gaussian process, disregarding the pilot tones and guard interval. [1] shows that the DVB-T signal is similar to band limited white Gaussian process.

5.2 Simulation of target

Figure 5.2 shows a Doppler delay plot of a simulated target. The reference and surveillance dataset are created by the DVB-T signal generator. The target is shown at $100Hz$ Doppler shift and $30km$ range. The direct signal is shown in zero Doppler and zero range. The rest of the ambiguities is generated by the signal coding due to the DSI.

These false target ambiguities are due to the pilots and the guard interval of the signal (see section 2 for definition). [1] discusses the code generated ambiguities, and methods to remove them.

5.3 Range walk in simulation data

This subsection will analyze range walk in the simulation data. As seen in section 4.3, range walk occur when the target moves through several range bins during the integration time. This is due to a large bistatic velocity compared to the bistatic range resolution of the PBR system. Range walk will cause energy dispersal in the correlation, and widening of the main lobe. The power is expected in the optimal case to increase with $3dB$ for each doubling in
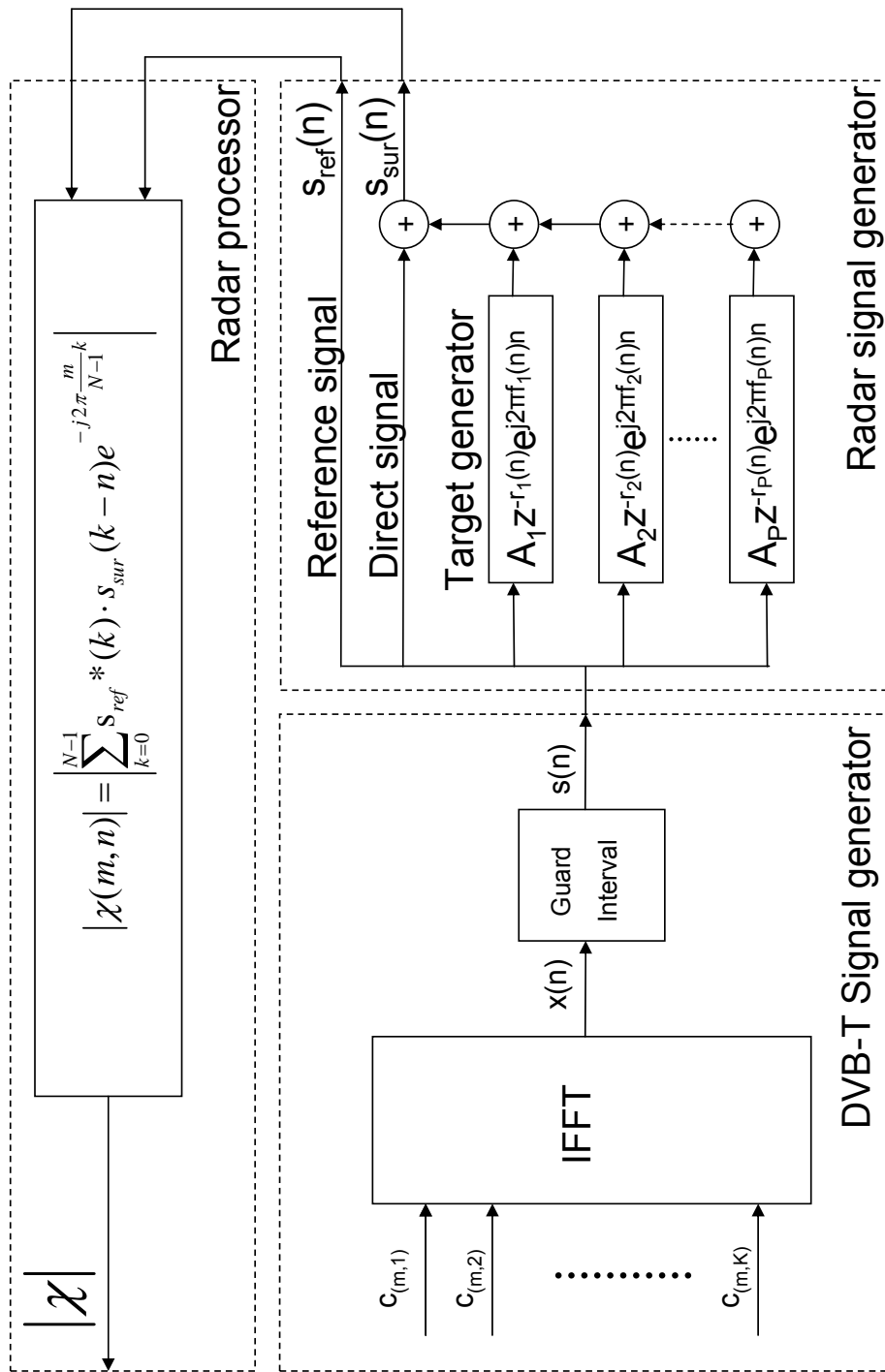
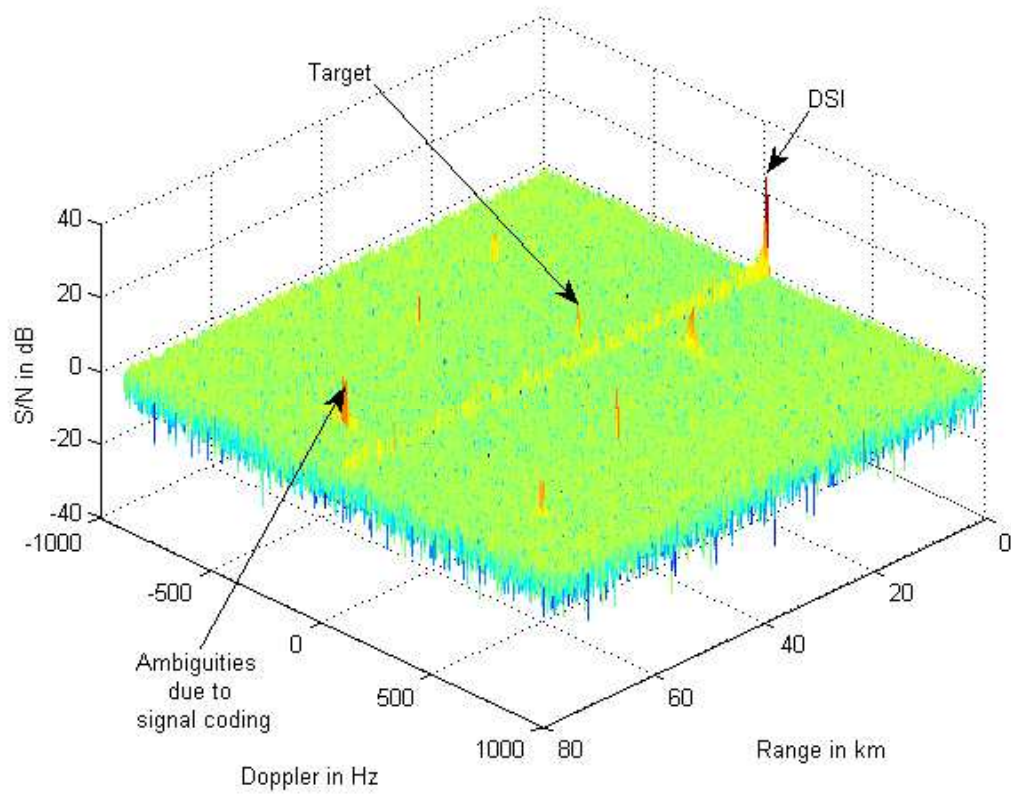*Figure 5.1:* Block diagram of the simulator

Figure 5.2: Doppler delay plot of target simulation

integration time (see section 1.2).

Figure 5.3 shows a cross section in range of a target with several different integration times, with no bistatic velocity. I.e. no range walk will occur for this target. This can be seen because there is no widening or movement of the main lobe when the integration time is increased. This is expected, because when the target experiences no bistatic velocity during integration time, no range walk occurs.

Figure 5.4 shows the (S/N) as a function of the integration time. The (S/N) from this plot was found by taking the maximum of the cross section for each integration time. The (S/N) increases with a number less than $3dB$ for each doubling of the integration time, but it is close for low integration times. The (S/N) does not increase with the theoretical $3dB$ because when the integration time increases, the Doppler resolution gets finer, and the energy is spread over more Doppler bins.

Figure 5.5 shows a cross section in range of the target with several different integration times, with a constant positive bistatic velocity during the integration interval. I.e. there will be some range walk for this target. The bistatic velocity used in this simulation is approximately $200m/s$, which is feasible for most airliners. We can see this because the main lobe widens and moves when increasing the integration time. This is expected, because when the target has a large enough bistatic velocity during the integration interval, there will be some range walk (see (4.4) for conditions on velocity for range walk to occur).

Figure 5.6 shows the (S/N) as a function of the integration time. The values were found by finding the maximum of the target Doppler cross section for each integration time. We see that the S/N increases more slowly than without range walk, and even drops after some threshold. The target main lobe clearly widens, and also there is a loss in energy. Range walk reduces the increase in $(S/(N)$ for large integration times.

5.4 Doppler walk in simulation data

This subsection will analyze Doppler walk in the simulation data. As seen in section 4.4, Doppler walk occurs when the target moves through several Doppler bins during the integration interval. This is due to a large bistatic acceleration and fine Doppler resolution of the system. Doppler walk leads to energy dispersal in the correlation and widening of the target response.

Figure 5.7 shows a cross section in Doppler with several different integration times, with no Doppler walk. The bistatic acceleration is zero.
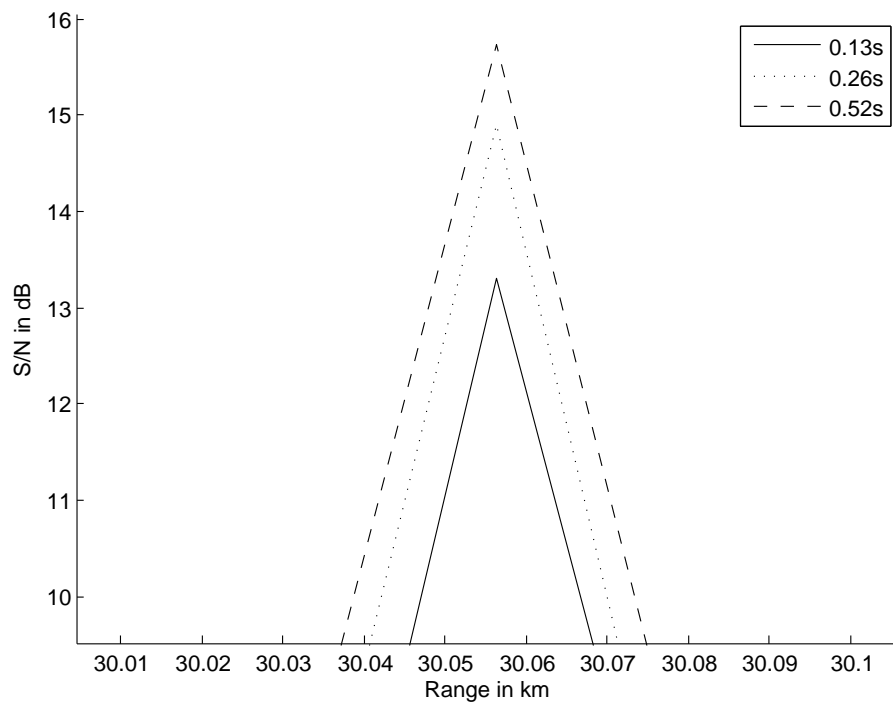
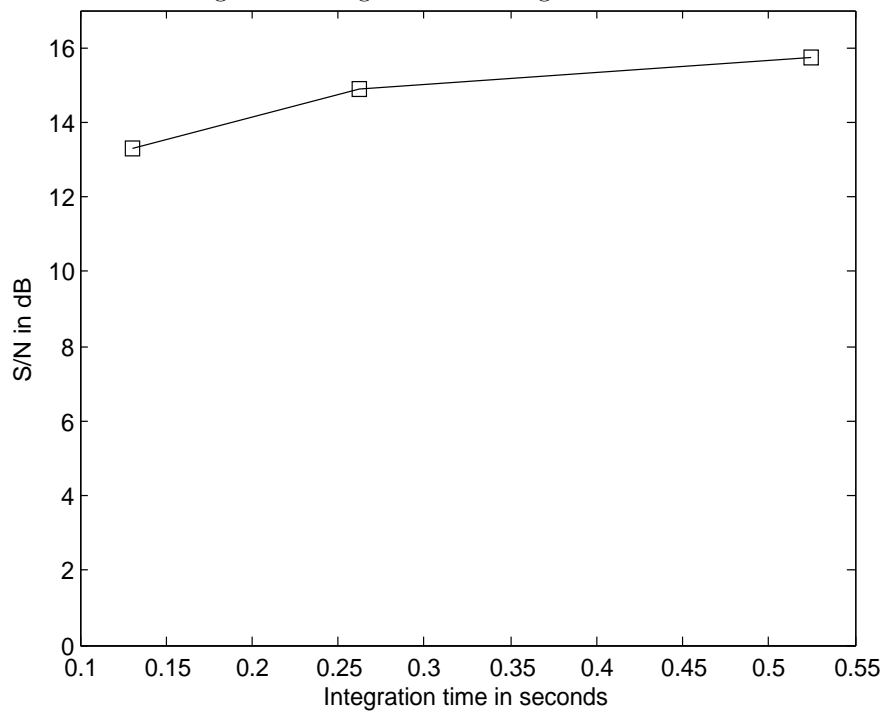*Figure 5.3:* Cross section in range of the target with no range walk

Figure 5.4: S/N as a function of integration time, no range walk
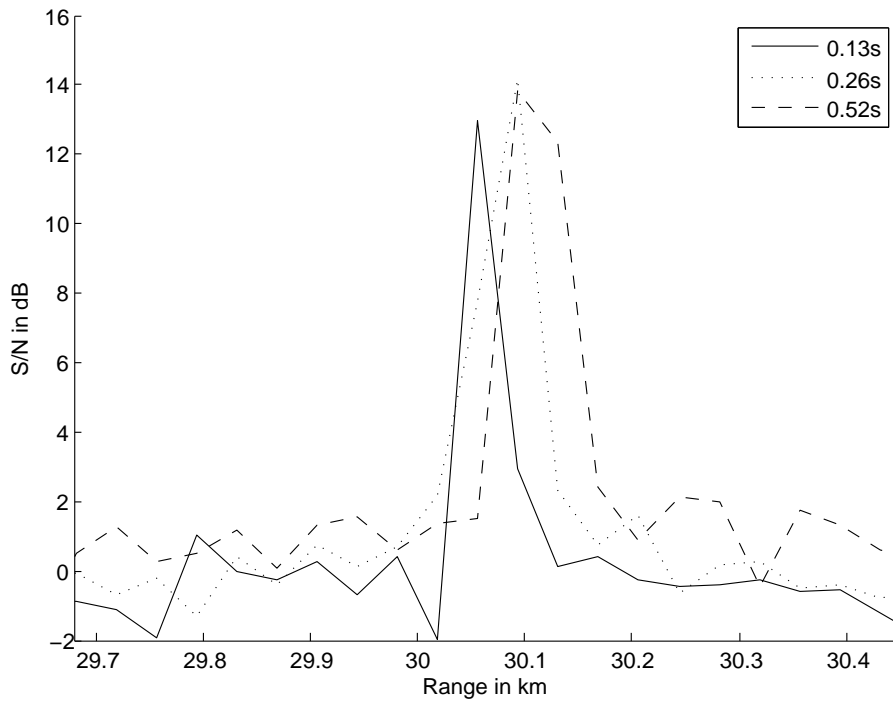
Figure 5.5: Cross section in range of the target, where the effects of range walk is apparent. The target response is widening and the energy is dispersed.
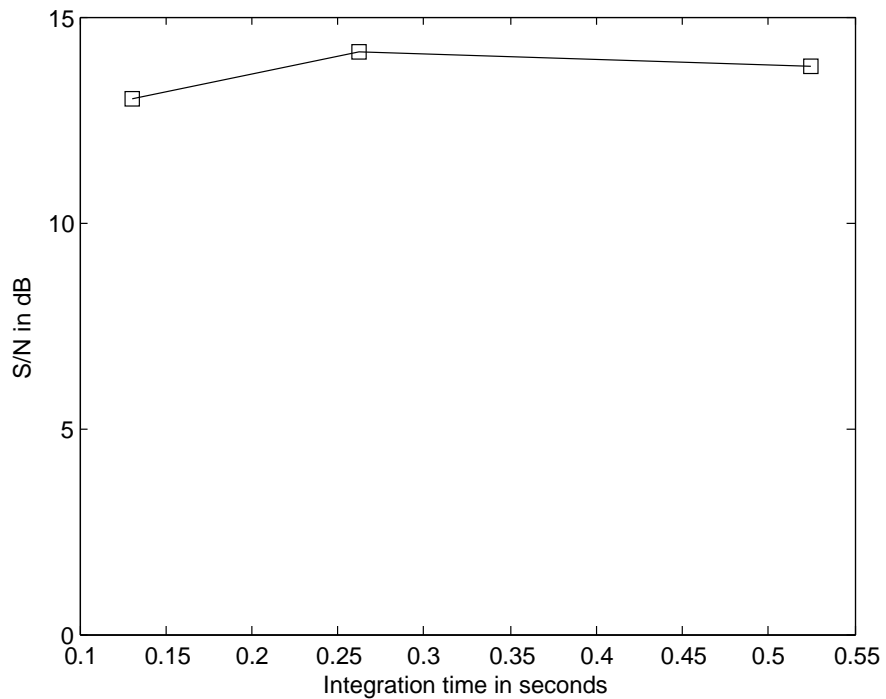

Figure 5.6: S/N as a function of integration time, displaying the effects of range walk on (S/N)

Figure 5.8 shows the (S/N) as a function of the integration time. The values were found by finding the maximum of the target Doppler cross section for each integration time. We see that the (S/N) increases when the integration time increases, but it does not increase with $3dB$ for each doubling in the integration time. This occurs because when the integration time increases, the Doppler resolution increases and the energy is spread over more Doppler resolution cells.

Figure 5.9 shows a cross section in Doppler of the target with several different integration times, with a non-zero bistatic acceleration. The bistatic acceleration is approximately $39.24m/s^2$ which is four times the gravity, given that the center frequency is $500MHz$. The main lobe is widening and moving as the integration time increases.

Figure 5.10 shows the (S/N) as a function of the integration time. The values were found by finding the maximum of the target Doppler cross section for each integration time. The (S/N) does not increase as fast as in the no Doppler walk case, and actually drops when increasing the integration time over a threshold. This causes energy dispersal in Doppler, and lower the Doppler resolution of the system.
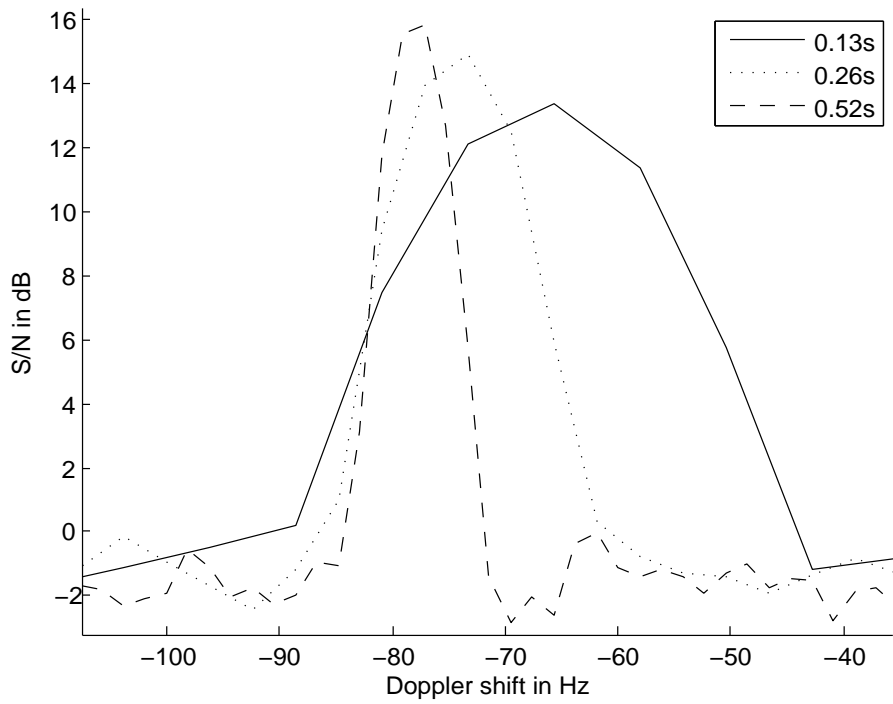
Figure 5.7: Cross section in Doppler of the target with no Doppler walk
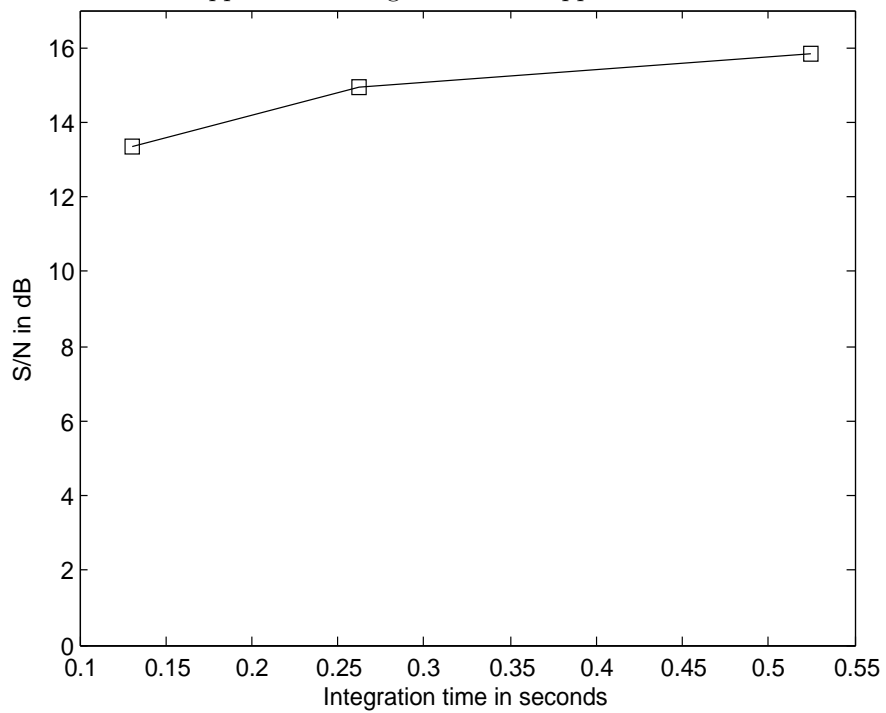

Figure 5.8: S/N as a function of integration time, no Doppler walk is occuring
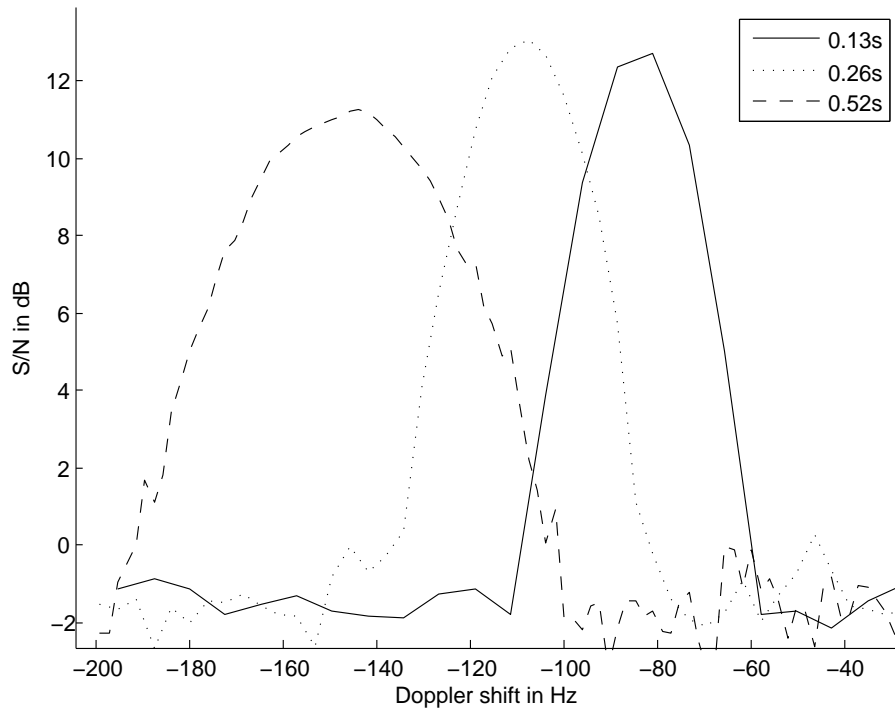
45

Figure 5.9: Cross section in Doppler of the target where the effects of Doppler walk is apparent. The target response is widening and the energy is dispersed.
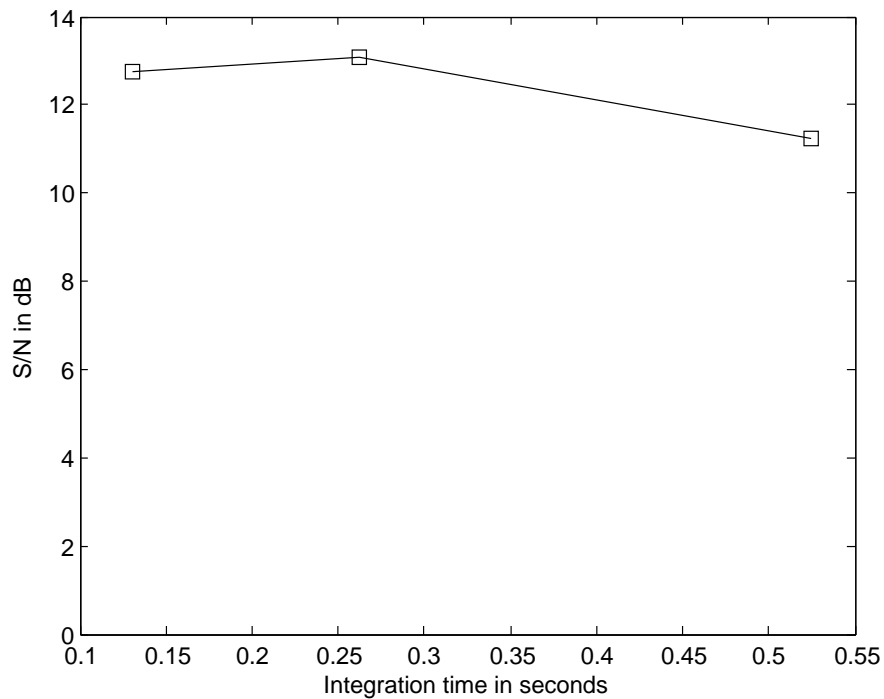

Figure 5.10: S/N as a function of integration time, displaying the effects of Doppler walk on (S/N).

5.5 Results of the simulations

As seen in the last subsections, range and Doppler walk have an effect on the correlation in a simulated DVB-T based PBR. The (S/N) drops when increasing the integration time (Figure 5.6 and 5.10), and the target response spreads in range and Doppler. The effect of increasing the integration time is in the optimal case an increase of approximately $3dB$ of the (S/N) for each doubling of the integration time.

The range walk simulation was done with a target having bistatic velocity of $200m/s$. This is feasible for most airliners. In other words, range walk is expected to be a problem for a standard DVB-T based PBR system. But the Doppler walk simulation was done with a bistatic acceleration of four times the gravity, which is a high value. Pilots cannot hold this acceleration for very long because of discomfort and even fainting. But there exist trajectories where the plane can produce bistatic acceleration, but not experience acceleration itself. This is a consequence of the bistatic geometry. I.e. there are trajectories where the bistatic acceleration can be large, and the acceleration the target experiences is small. These trajectories are only a small subset of all possible trajectories, so the problem of Doppler walk will most probably be a rare phenomenon.

The simulations show that range and Doppler walk pose problems for a DVB-T based PBR system. Real data will be analyzed next to see if the real data shows the same problems as with the simulated targets.

6 Experimental setup

The processing method used in this setup is the implementation of the Ambiguity Function. It is implemented in MATLAB, and is based purely on $FFT/IFFT$ and complex multiplications. It is therefore an efficient processing method to create Doppler-delay matrices. This section will present some experimental data.

6.1 PBR setup, using ADS-B data as reference

The PBR setup uses ADSB data as a source of reference. Figure 6.1 shows an accumulated Doppler-delay plot, with ADS-B data plotted on top. Since many airplanes still are using IMU's instead of GPS (Global Positioning System) in the ADSB system, the accuracy is not necessarily good. The IMU's drifts during flight time, and may give a position with very low accuracy.
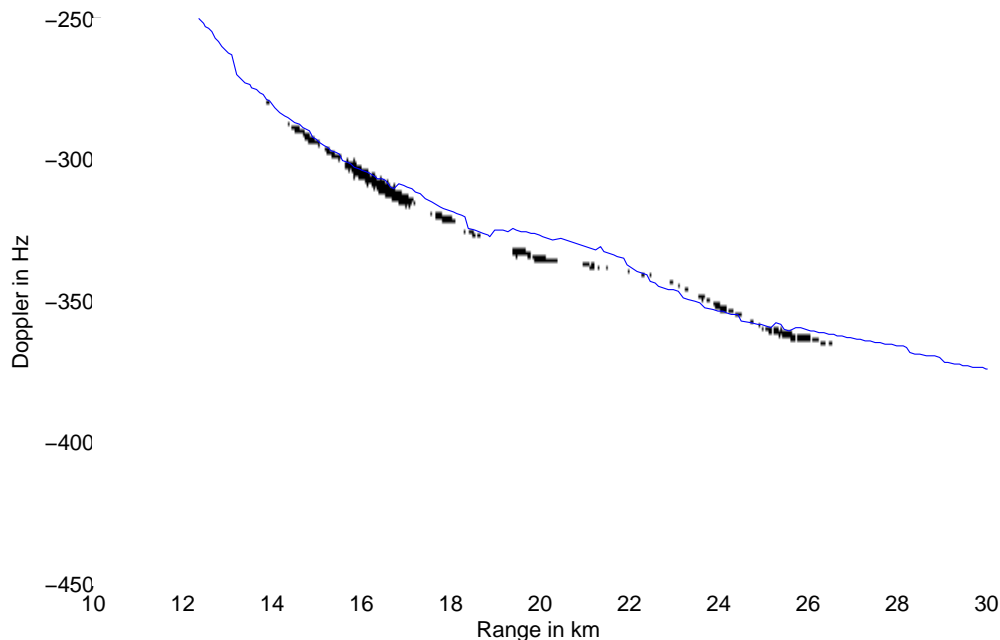

Figure 6.1: Doppler delay plot, with ADSB data, where the blue line is ADS-B data.

6.2 Passive bistatic radar geometry and setup

This subsection will present two bistatic setups with FFI/Kjeller as receiver site. Figure 6.2 displays the geometry of the two setups.

The center frequencies for the UHF channels used in the next tables are given in table 2.3.

The first setup uses Tryvasshoegda as transmitter site, and the parameters for this bistatic setup are given in table 6.1.
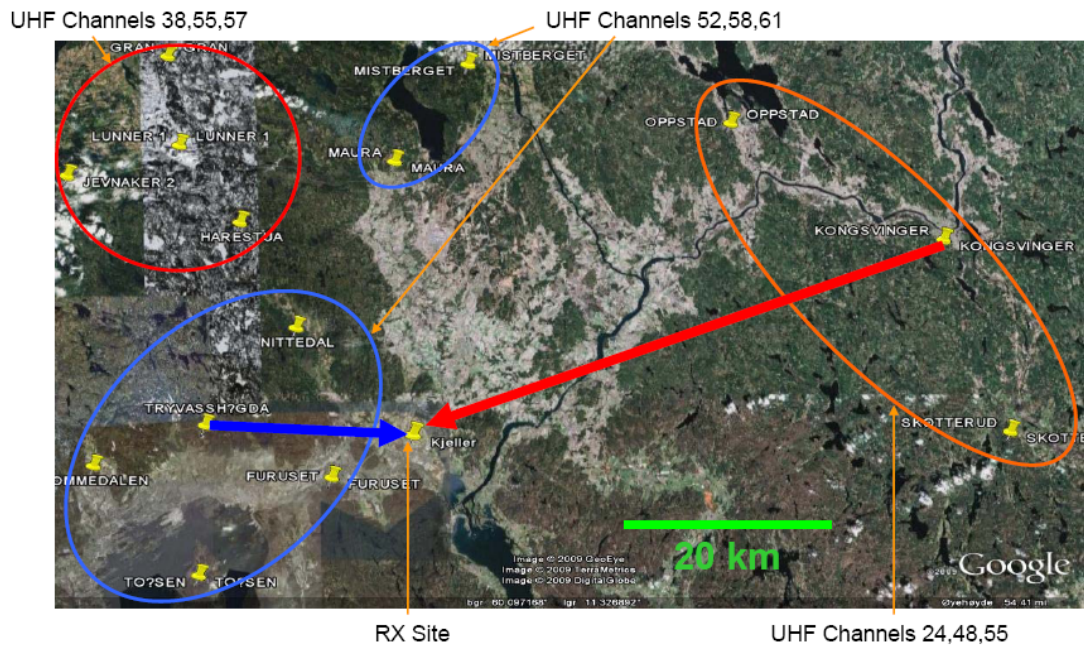
Figure 6.2: Bistatic setup, displaying the two transmitters used and the receiver at FFI/Kjeller

L	$20.44km$
Max e.r.p.$(G_T P_T)$	$45.3dB$
Diffraction loss (F_T^2)	$30dB$
MUX1	UHF Channel 52
MUX2	UHF Channel 58
MUX3	UHF Channel 61

Table 6.1: Table of parameters for bistatic setup, with Tryvasshoegda as transmitter and FFI/Kjeller as receiver

A plot displaying the diffraction loss between Tryvasshoegda and FFI/Kjeller is given in figure 6.3 (a). These diffraction plots were produced with the algorithm of ITU-R P.526-10 "Propagation by diffraction". The terrain is generated from DTED (Digital Terrain Elevation Data) level 1, which roughly has a Cartesian grid resolution of 90m by 90m, resulting in varying longitudal resolutions. The interval latitude is 3 arc seconds, while the interval longitude 6 arc seconds in southern Norway.

The second setup uses Kongsvinger as transmitter site, and the parameters for this bistatic setup is given in table 6.2.

L	$57.39km$
Max e.r.p. $(G_T P_T)$	$46.9dB$
Diffraction loss (F_T)	$50dB$
MUX1	UHF Channel 24
MUX2	UHF Channel 48
MUX3	UHF Channel 55

Table 6.2: Table of parameters for bistatic setup, with Kongsvinger as transmitter and FFI/Kjeller as receiver

A plot displaying the diffraction loss between Kongsvinger and FFI/Kjeller is given in figure 6.3 (b).

We see that the diffraction loss for the PBR setup using Tryvasshoegda is approximately $30dB$, and the distance L is $20.44km$. The power density at FFI/Kjeller is

$$\Phi_{Tryvasshoegda} = \frac{P_T G_T}{4\pi L^2} F_T^2 = -81.9dB \tag{6.1}$$

The diffraction loss for the PBR setup using Kongsvinger is approximately $50dB$, and the distance L is $57.39km$.

$$\Phi_{Kongsvinger} = \frac{P_T G_T}{4\pi L^2} F_T^2 = -109.3dB \tag{6.2}$$

The difference in power density at FFI/Kjeller using the Kongsvinger and Tryvasshoegda is $\Phi_{Kongsvinger} - \Phi_{Tryvasshoegda} = 27.4dB$. We will see in the following subsections that this extra direct signal loss is vital when processing the experimental data.
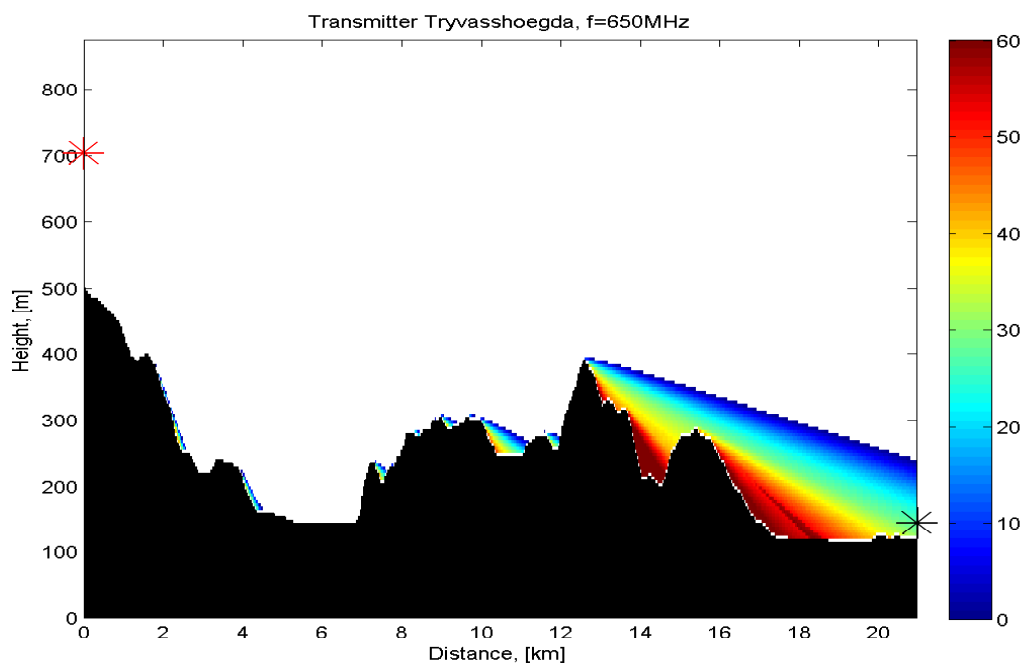
(a) Diffraction between Tryvasshoegda and FFI/Kjeller.
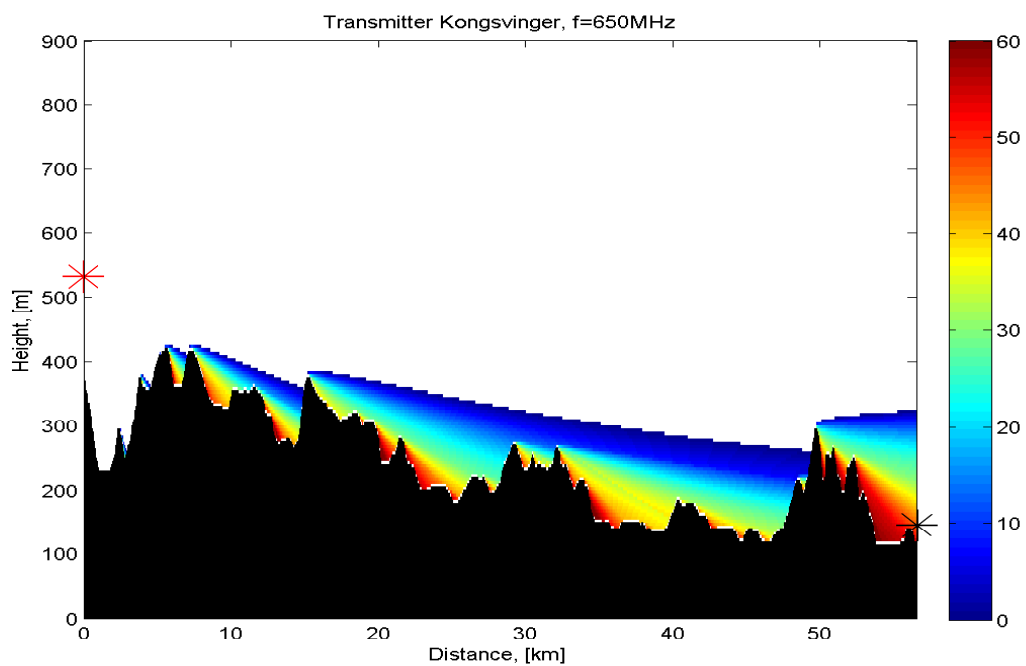
(b) Diffraction between Kongsvinger and FFI/Kjeller.

Figure 6.3: Diffraction loss between transmitter and reciever, given in *dB*.

6.3 Processing of experimental data using Tryvasshoegda as transmitter

The setup for the recording presented in this section is given in figure 6.4. The radar recording captures an airliner in approach at Gardermoen. The plane passes the receiver site at close range, and also passes the extended baseline. An accumulated Doppler-delay plot with close up of a target and cross sections both in Doppler and range is given in figure 6.5. The cross sections also shows the signal strength in relation to the noise floor. The problem with using Tryvasshoegda as the transmitter of opportunity is the direct signal interference. From figure 6.3 (a), the diffraction loss from Tryvasshoegda to FFI is approximately $30dB$. The transmitter has a large transmitter power, and the surveillance antenna used in the setup struggles with too much DSI (Direct Signal Interference). The next subsection will show a better suited setup for this area.
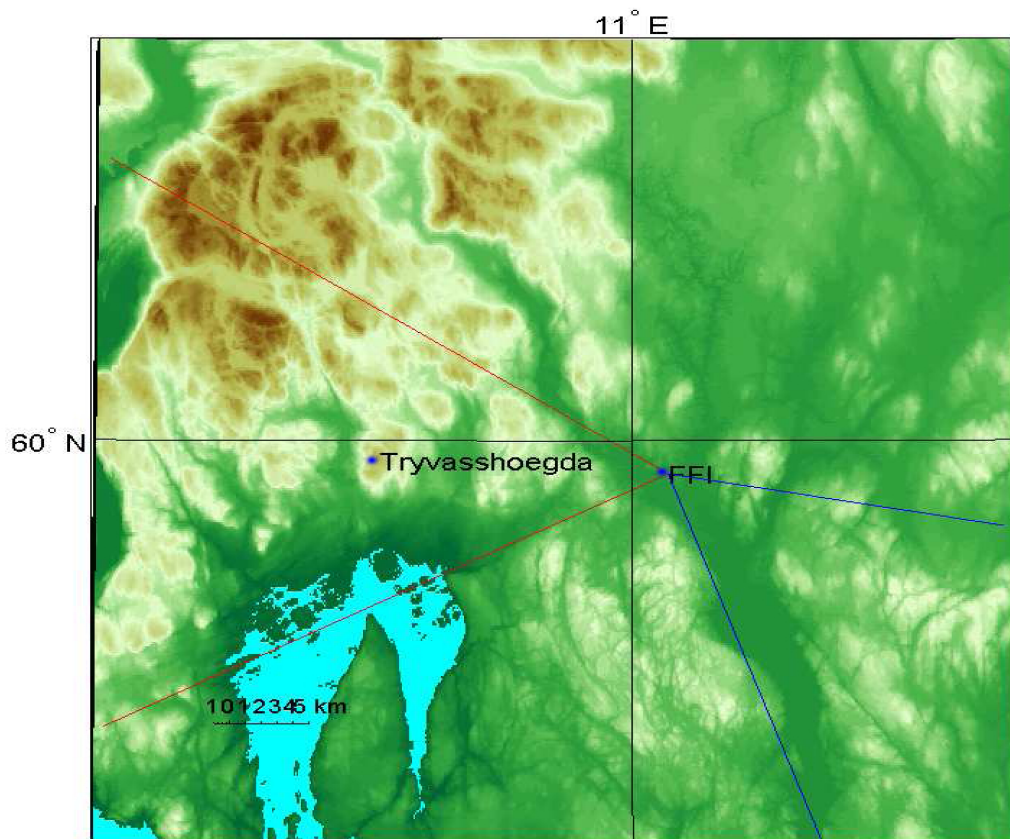

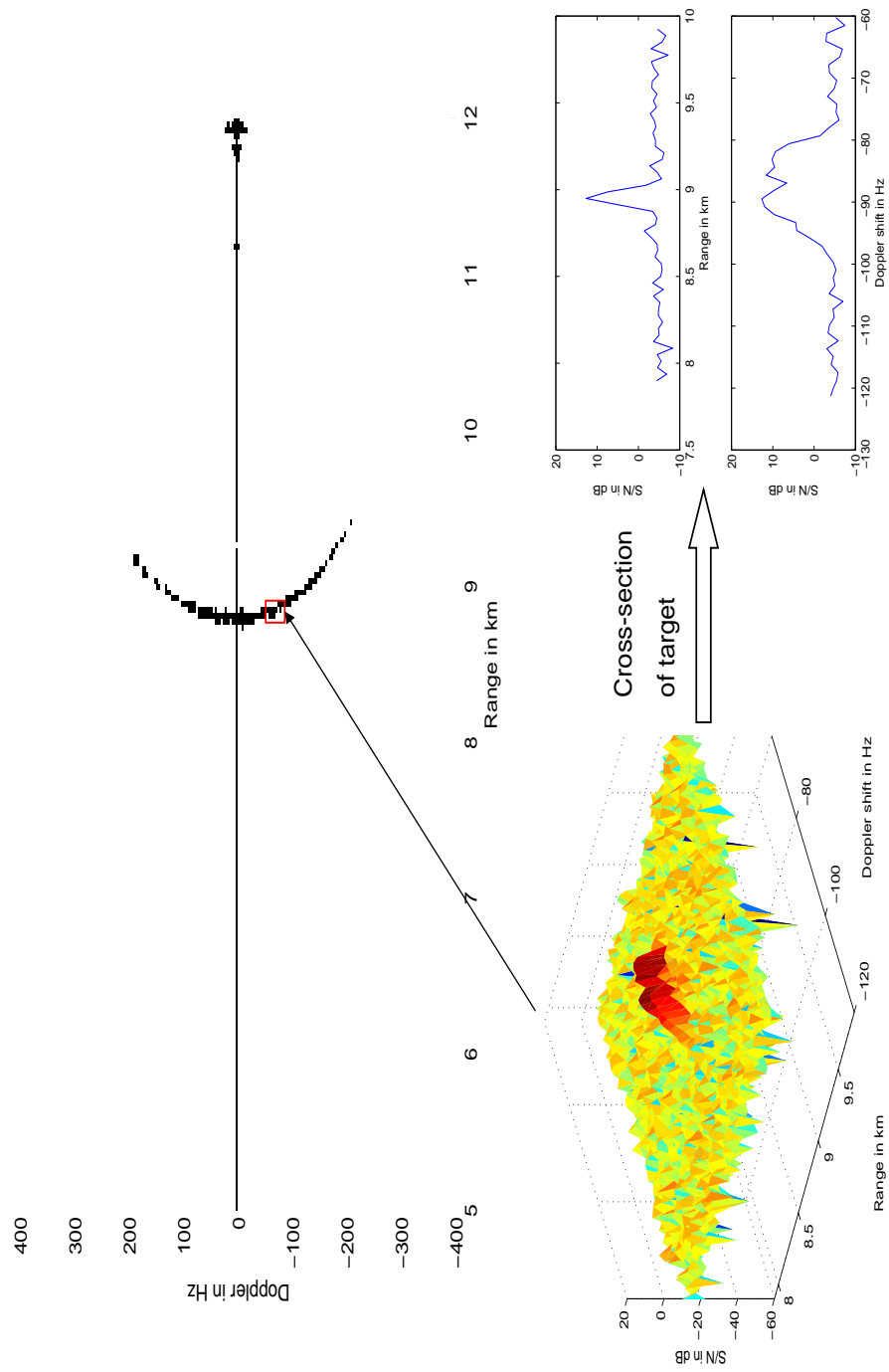*Figure 6.4:* Bistatic geometry of Tryvasshoegda and FFI/Kjeller

Figure 6.5: Doppler-delay of target with bistatic geometry given in figure 6.4, integration time 0.79s

6.4   Processing of experimental data using Kongsvinger as transmitter

The setup for the recording presented in this section is given in figure 6.6.

The radar recording captures an airliner climbing from the takeoff at Gardermoen. The plane is approaching the receiver, so it has negative Doppler shift throughout the recording. An accumulated Doppler-delay plot with close up of a target and cross sections in both range and Doppler is given in figure 6.5. The cross sections also show the signal strength in relation to the noise floor. This setup has shown to be better suited than the Tryvasshoegda setup. From figure 6.3 (b), the diffraction loss from Kongsvinger to FFI/Kjeller is $50dB$ which is $20dB$ more loss in DSI than Tryvasshoegda. The DSI is not so severe using Kongsvinger as transmitter of opportunity. This setup is the main setup used in the rest of the work.
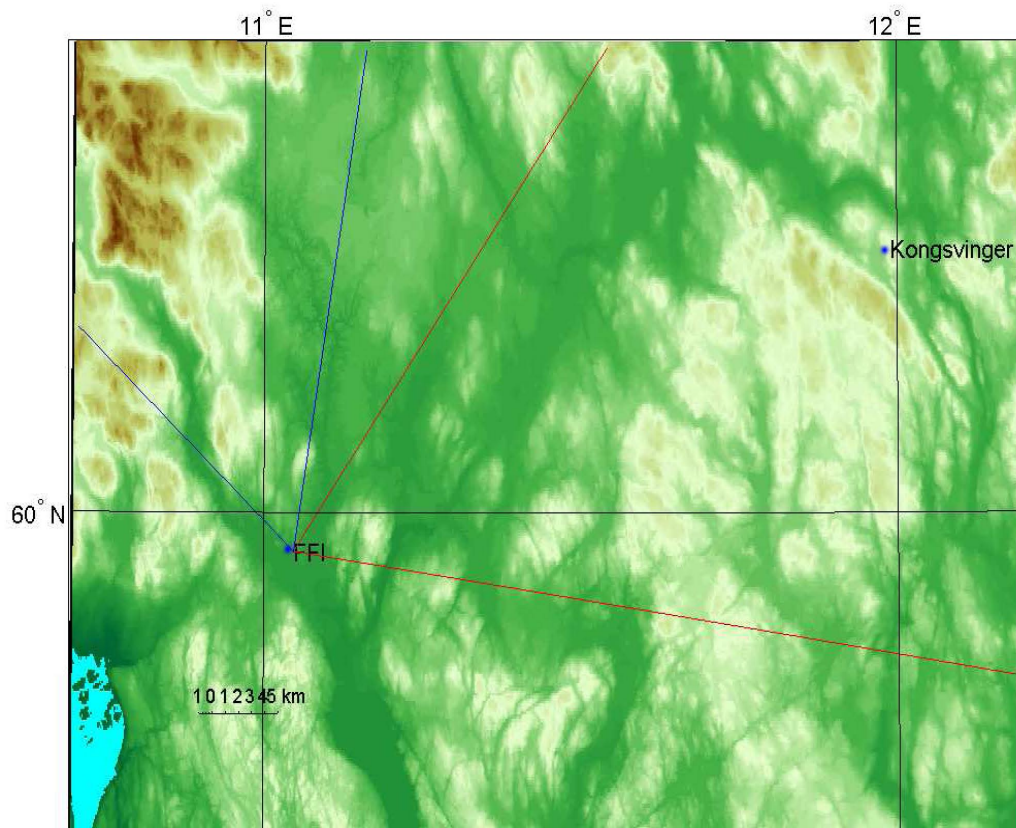

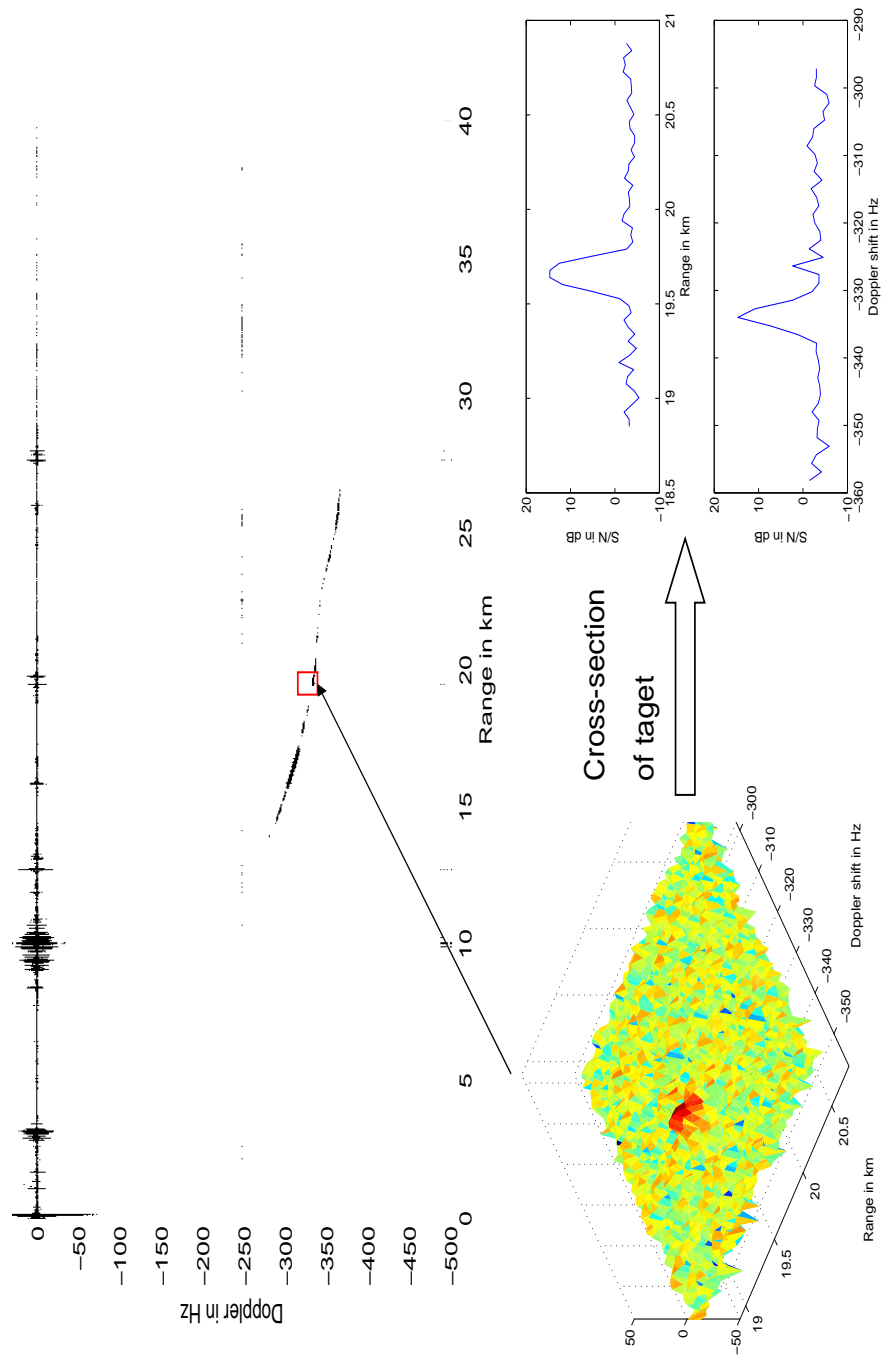*Figure 6.6:* Bistatic geometry of Kongsvinger and FFI/Kjeller

Figure 6.7: Doppler-delay of target with bistatic geometry given in figure 6.6, integration time 0.79s

7 Results from real data analysis

We have seen from the simulations that range and Doppler walk may pose problems using long coherent integration intervals. This section will analyze real data with emphasis on the effects of range and Doppler walk.

7.1 Range walk

Range walk is defined in section 4.3. A target with bistatic velocity of approximately $105m/s$ will be analyzed, and the UHF channel is 24. This gives us from (4.4) that when $T_I > 0.36s$, range walk will occur. When the integration time is smaller than $0.36s$, range walk may occur.

Figure 7.1 shows an accumulated Doppler-delay plot with two target cross sections in range at different positions. The target cross sections widen when the integration time is increased, and it is clear that range walk does occur.

Figure 7.2 (a) shows a cross section in range of the target given in the accumulated Doppler-delay plot from figure 7.1. The cross section is given for different integration times, and the main lobe of the target widens when integration time increases. Also, (S/N) increases for each doubling of the integration time until it reaches $0.26s$. The next doubling in integration time actually decreases the (S/N) and the target response widens, and the result of range walk is apparent. This is accurate with the fact pointed out that for $T_I > 0.36s$, range walk will occur.

Figure 7.2 (b) shows the maximum (S/N) for the target for each integration time from figure 7.2 (a). The (S/N) is expected by the bistatic radar equation (1.1) to increase by $3dB$ for each doubling of the integration time.

It is apparent that range walk affects the coherent integration for the target given in this section. The effects are smaller (S/N) and a wider target response when increasing the integration time over a certain threshold, which in this case is $T_I > 0.36s$. For targets with a larger bistatic velocity, a smaller limit on the integration time is expected.

Figure 7.1: Accumulated Doppler-delay plot, and cross section in range at different integration times of the target at different positions
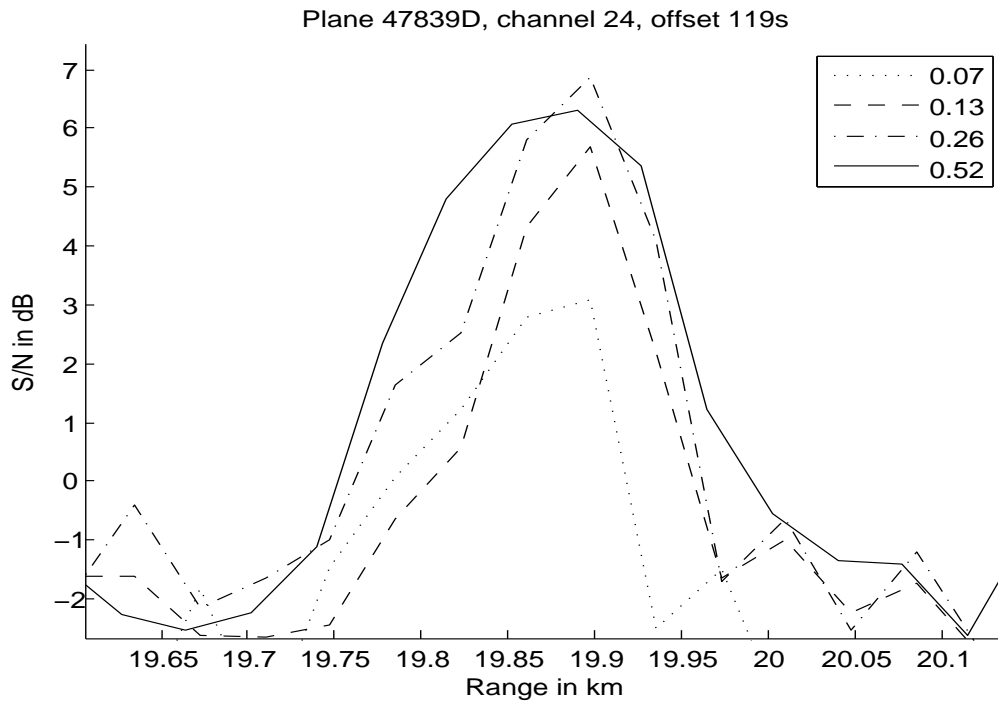
(a) Cross-section in range for different integration times, showing the widening of the target response in range
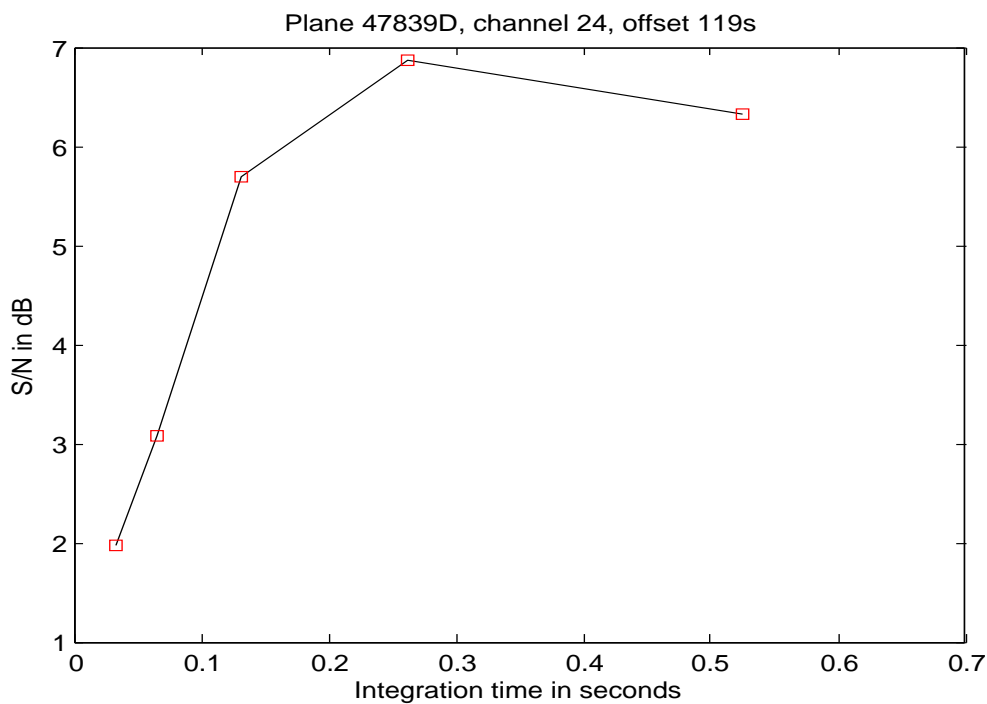
S/N as a function of integration time, showing the effects of range walk on (S/N).

Figure 7.2: Figure displaying the effects of range walk. The target response is widened, and the (S/N) gain when increasing the coherent integration time is not as large as theoretically expected

7.2 Doppler walk

Doppler walk is defined in section 4.4. Doppler walk occurs when the target's bistatic acceleration is large compared to the integration time and Doppler resolution. This results in that the target moves over several Doppler bins during the integration time. Effects of Doppler walk is lower (S/N) and widening of target response.

Figure 7.3 shows a Doppler-delay plot of target passing the extended baseline, and cross sections in Doppler of the target in two positions. The cross section plots show the target cross section in Doppler for two different integration times. The target response widens and the (S/N) drops when the integration time increases. These are two examples of Doppler walk.

Figure 7.3 (a) displays a cross section in Doppler of the target given in figure 7.3 for different integration times. (S/N) does not increase when doubling the integration time, but actually drops. Figure 7.4 (b) displays the maximum (S/N) for each integration time from figure 7.3 (b). Here it is apparent that the (S/N) drops when increasing the integration time.

The consequence of Doppler walk is clearly illustrated in the two last plots. The main lobe widens and gives no gain in Doppler resolution when increasing the integration time. The Doppler resolution is doubled when the integration time doubles (1.9). But when Doppler walk occur, the target is spread over more Doppler resolution cells and the (S/N) drops.
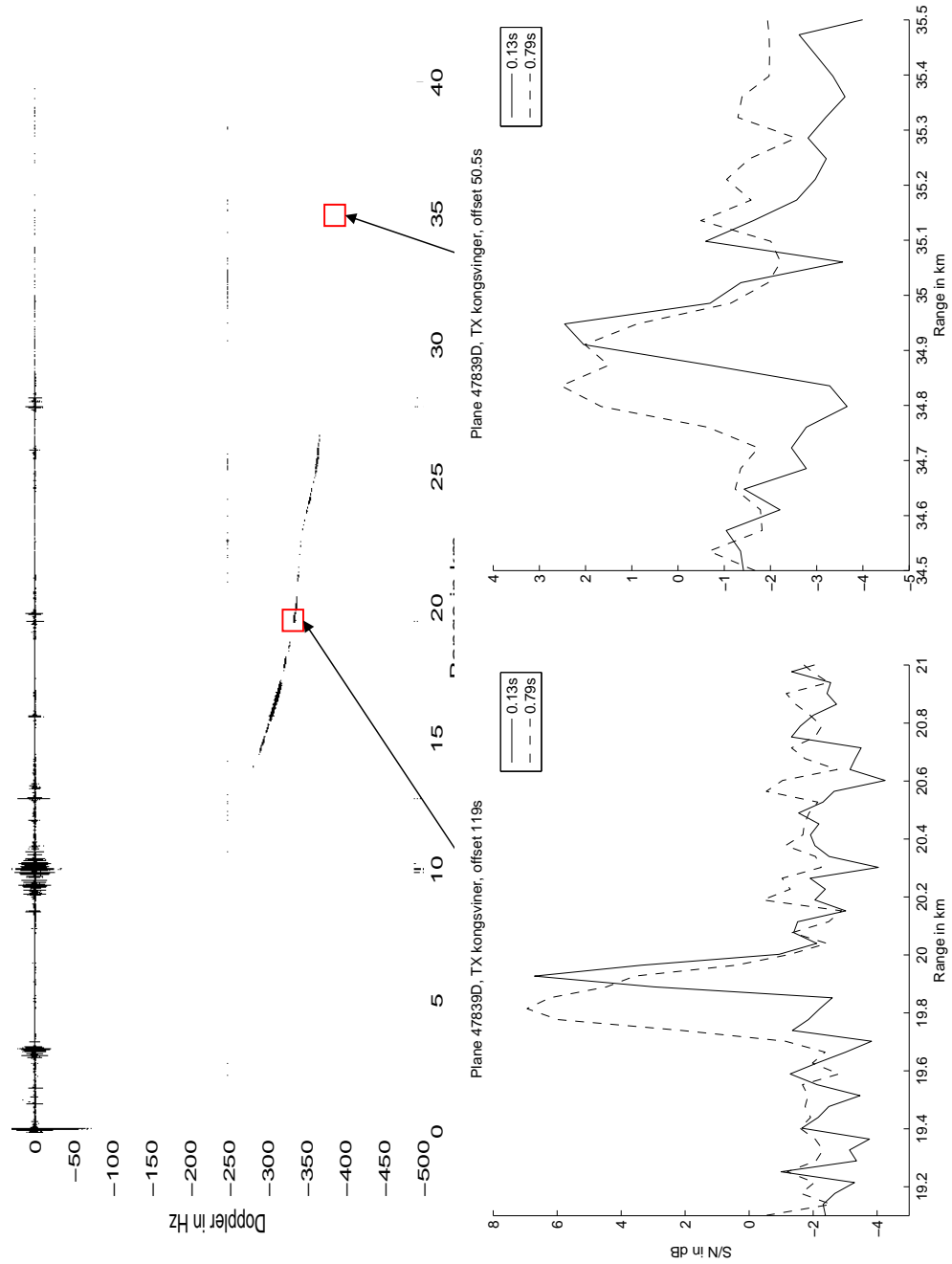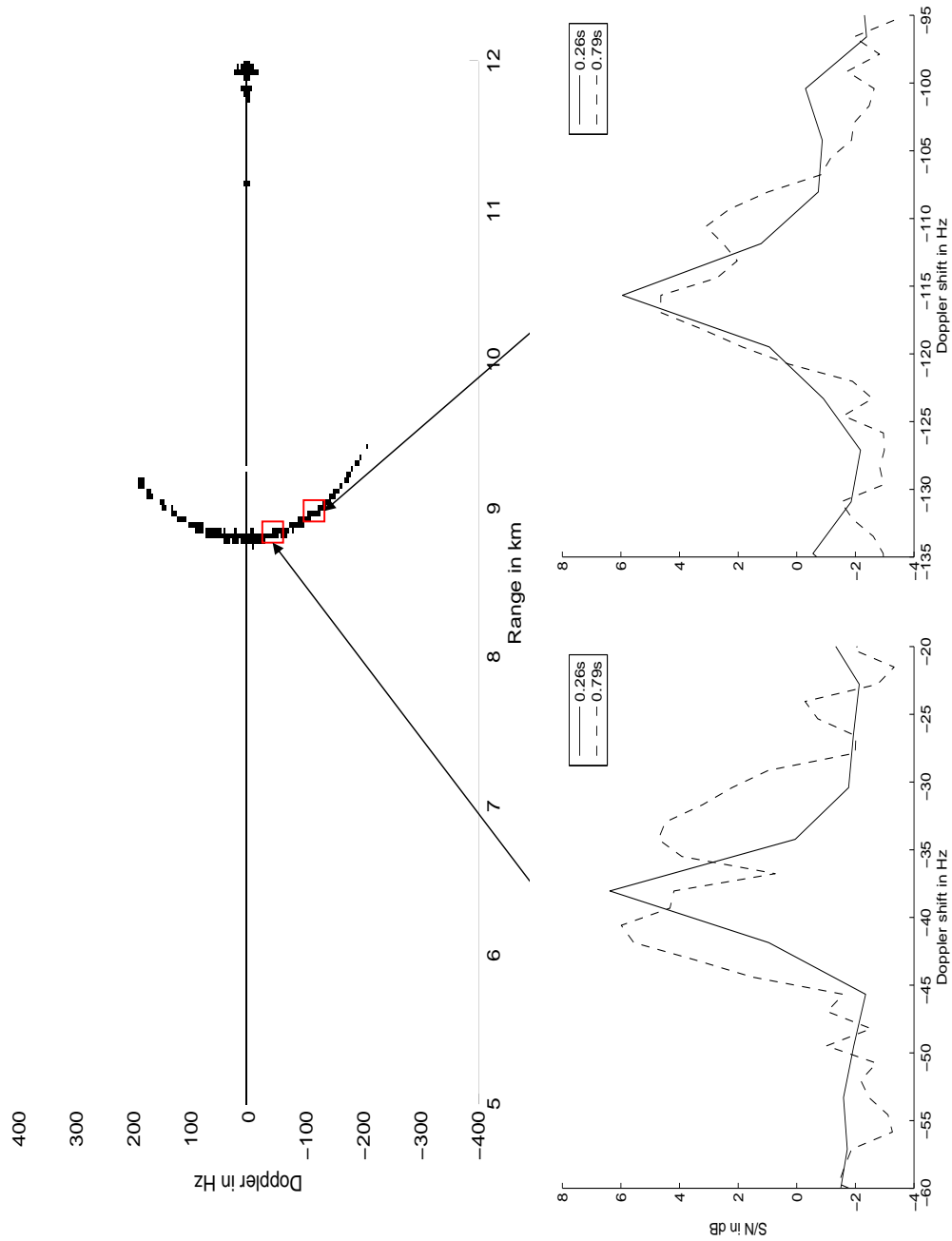
Figure 7.3: Accumulated Doppler-delay plot, and cross section in Doppler shift at different integration times of the target at different positions
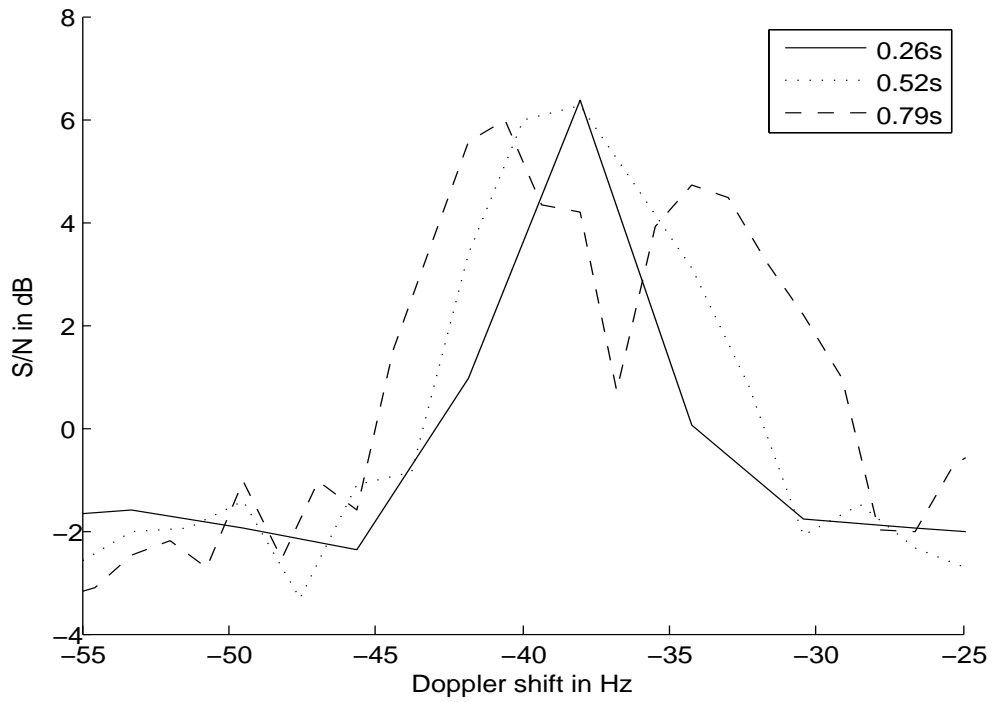
(a) Cross-section in Doppler shift for different integration times, showing the widening of the target response due to Doppler walk
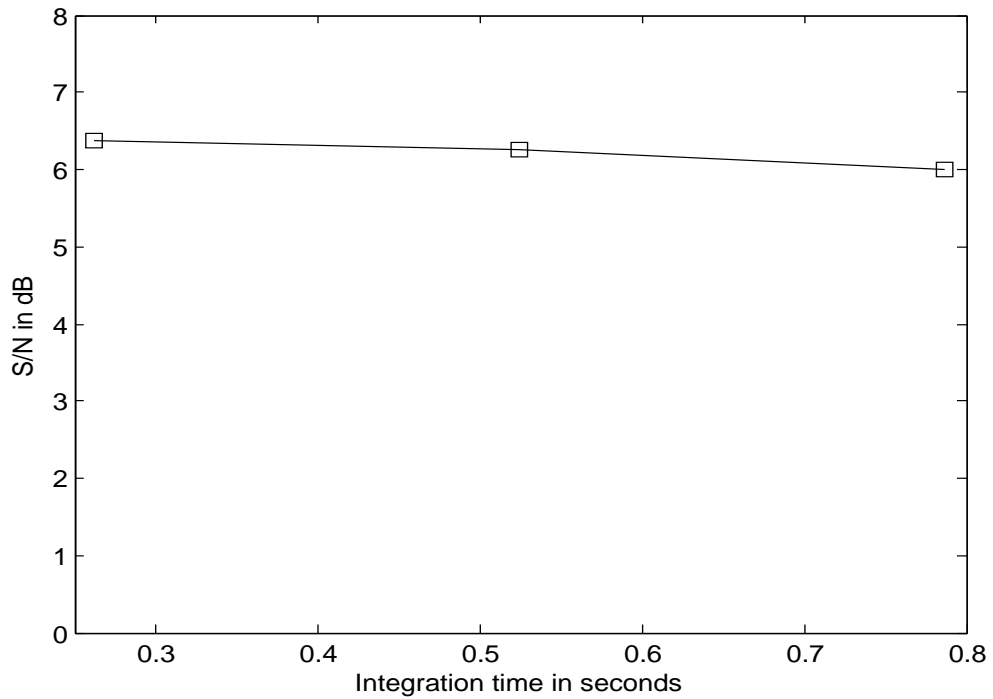
(b) S/N as a function of integration time, showing the effects of Doppler walk on (S/N).

Figure 7.4: Figure displaying the effects of Doppler walk. The target response is widened, and the (S/N) gain when increasing the coherent integration time is not as large as theoretically expected

7.3 Discussion of range and Doppler walk

The last two subsections presented the effects of range and Doppler walk on real targets for a DVB-T based PBR system. The consequences of range and Doppler walk are that the gain of increasing the integration time, which is higher (S/N), does not occur. There is actually loss in peak (S/N) and widening of the target response. These are problems that will arise in a DVB-T based PBR system.

The consequences of range and Doppler walk are smaller probabilities of detection. Long integration times are wanted in these types of systems to increase the (S/N). But the inequalities (4.4) and (4.6) set the limit of when range and Doppler walk occurs. One possibility is to set a series of parameters for the potential radar system, and choose an integration time based on this. But this is a sub-optimal solution to this problem. For example, the optimum integration time for the target given in figure 7.1 is approximately $0.3s$. This gives the highest gain in (S/N), and only a small loss in range resolution.

To find an optimal integration time for each radar system is a solution, but does not necessarily give the wanted gain in (S/N). Also, it might not give the Doppler resolution required for the radar system.

An example of Doppler walk was actually hard to find with this radar system. Doppler walk demands large bistatic accelerations, and this was rare in my experience with this system. Since the only targets analyzed were airliners, large bistatic velocities and accelerations were not expected. But faster planes such as jet fighters are expected to have larger bistatic velocities and accelerations, and are therefore more probable to cause Doppler walk.

Bistatic acceleration can occur even when the airplane experiences no acceleration. This is a product of the bistatic geometry. For example, the target path displayed in the accumulated Doppler-delay plot in figure 7.3 has a small acceleration in the Cartesian reference frame, but has a large bistatic acceleration in the bistatic plane. Actually large enough to induce Doppler walk. But these trajectories are quite few compared to possible trajectories. Almost all airborne targets have the velocity needed to give range walk in a DVB-T based PBR system. This is due to the high resolution given by the large bandwidth of the DVB-T signal. Therefore, range walk is considered to be a more likely problem than Doppler walk.

8 Possible solutions to range and Doppler walk in DVB-T based PBR systems

Range and Doppler walk might pose problems for DVB-T based PBR systems. The energy dispersal in the correlation due to range and Doppler walk can be extensive when the target has large bistatic velocity and acceleration. The following subsections will take a look at possible solutions to decrease the effects of range walk on the targets exhibiting large bistatic velocities.

8.1 Noncoherent integration and speed calibration

Noncoherent integration will increase (S/N) with $\sqrt{2}$ for each doubling of the integration time. This is less than the doubling in gain coherent integration gives. Both coherent and noncoherent integration are described in [5], p 44-45. But when range walk occurs, this gain will be reduced for both coherent and noncoherent integration. The case for coherent integration was shown in the last section. However, the bistatic velocity of the target is known due to the Doppler information. This information is not used to compensate for the loss due to range walk.

Next, a solution for increasing the (S/N) gain will be explained. Since the bistatic velocity is known, under an assumption of no bistatic acceleration, the (S/N) can be increased using noncoherent integration and speed calibration. If we call the coherent integration interval giving range walk T_I, we can piece the interval up in N pieces with integration time of $\frac{T_I}{N}$. We perform coherent integration on each of these integration intervals giving N coherent correlations, which we call $\chi_k(m,n)$ where $k = 0, ..., N-1$. We then give each $\chi_k(m,n)$ a range shift proportional to the bistatic velocity and time such that the new correlation is

$$\hat{\chi}_k(m,n) = \chi_k(m, n - [\frac{v_B}{\Delta R} k \hat{T}_I]) = \chi_k\left(m, n - [\frac{\lambda}{2\Delta R} km]\right) \tag{8.1}$$

where $\Delta R = \frac{c}{B}$ is the range resolution, $\hat{T}_I = \frac{T_I}{N}$ is the coherent integration time for each k, λ is the wavelength of the DVB-T signal and $[x]$ means the integer value of x. v_B is the bistatic velocity at point m in the correlation given in (1.8) and f_B from this equation is $f_B = \Delta f m = \frac{m}{T_I}$. The reason for this range shift is that for each noncoherent integration interval, the target will at each point m, move because of a non-zero bistatic velocity. Assuming no bistatic acceleration, the target will at each time $\hat{T}_I k$ be at a new range. If we call the starting range of the target R, the new range for each k and m will be $R + \frac{\lambda}{2} km$. This is the reason for range shifting the correlation for each k and m.

Standard noncoherent integration is given as

$$\chi_{IC}(m,n) = \sum_{k=0}^{N-1} |\chi_k(m,n)| \tag{8.2}$$

But if we sum together $\hat{\chi}_k(m,n)$ instead of $\chi_k(m,n)$, we get

$$\chi_{IC,speedcalib}(m,n) = \sum_{k=0}^{N-1} |\hat{\chi}_k(m,n)| \qquad (8.3)$$

This will give us an increase in (S/N) compared to standard noncoherent integration when range walk occurs. Figure 8.1 displays a cross section in range with the three different methods of integration for three different values of N for a simulated target. It has a bistatic velocity of $350m/s$ and starts at range of $30km$, and we can see from the figure that range walk is occurring. For $N = 8$, the non-coherent integration method with speed calibration shows the same (S/N) as the coherent integration method, but the accuracy is better. For $N = 4$, the non-coherent with speed calibration integration method shows improvement over the coherent integration method in the sense that the (S/N) is higher and the accuracy is better. But for $N = 2$, the non-coherent integration method shows little improvement compared to for $N = 4$, and the limit of the coherent integration interval $\hat{T}_I = \frac{T_I}{N}$ for each integration in the non-coherent integration is reached. When $\hat{T}_I$ does not satisfy (4.4), range walk occur for each of the coherent integrations in the non-coherent integrations, so there is little gain in using the method. So for $N = 4$, this method shows improvements on the simulated high bistatic velocity target.

Figure 8.2 displays a cross section in range for the target used in the analysis of range walk in section 7.1, for the three different methods of integration for three different values of N. In the figure for $N = 8$, the coherent integration method is superior to both of the non-coherent methods. This is because of the low (S/N) in each of the coherent integrations in the non-coherent integration methods produce. But for $N = 4$, the non-coherent integration with speed calibration has larger (S/N) than the two other methods. And for $N = 2$, the non-coherent integration with speed calibration is most efficient. This is because of the coherent integration time causing range walk is larger than $\hat{T}_I$, and therefore no range walk is occurring for the coherent integration intervals for the non-coherent integration. The (S/N) maximized for the non-coherent integration with speed calibration method for this bistatic velocity.

This method showed improvement over standard coherent integration, due to the fact that range walk occurs for the integration time. Doubling the integration time from $0.26s$ to $0.52s$ did not yield any gain. But when using the method of non-coherent integration and speed calibration described above, we get the expected $1.5dB$ gain in (S/N) given by non-coherent integration without range walk. This is illustrated in figure 8.3, where (a) shows coherent integration with integration time of $0.26s$ and $0.52s$, and (b) shows coherent integration time of $0.26s$ and non-coherent integration time with $\hat{T}_I = 0.26s$. Here, we clearly see the gain in using the method of non-coherent integration with speed calibration. The bistatic velocity of the target is low, i.e. that the range walk only shows significance at integration times larger than $0.3s$, the gain is only clear when doubling the integration time

from $0.26s$ to $0.52s$. But for targets with higher bistatic velocities, this method may show greater advantages.

One solution to maximize the (S/N) is to use a combination of coherent integration and non-coherent integration with speed calibration. Range walk is estimated to occur for bistatic velocities and integration times according to inequality (4.4). Therefore, regions in the Doppler-delay matrix giving range walk can be estimated, and different regions can use different integration methods. For a DVB-T based PBR system using UHF channel 24, coherent integration can be used for Doppler shift given by $|f_B| < 240Hz$. Non-coherent integration with speed calibration and $N = 2$ can be used for $240Hz \leq |f_B| < 480Hz$. And $480Hz \leq |f_B| < 960Hz$. In this way, a sub optimal, but more efficient method than coherent integration for all f_d can be developed for each PBR system. The only variable is the bandwidth and the center frequency, so a standard method for a DVB-T based PBR system can be used.

This method gives no gain in (S/N) for targets experiences Doppler walk. But as mentioned in section 7.3, Doppler walk is more rare that range walk. This method gives a cruder Doppler resolution than with coherent integration because of shorter coherent integration times.

## 8.2   Reduction of the effects of Doppler walk

Since the range-Doppler processing give Doppler information, and therefore knowledge of the bistatic velocity it is possible to counteract the effects of range walk as discussed in the last subsection. But there is no knowledge of the bistatic acceleration, and it is therefore difficult to counteract the effects of Doppler walk.

But after a target has been detected, and the tracker is locked on to a target, bistatic acceleration may be estimated. And this information can potentially be used in an adaptive processing scheme. Since this work has not studied the problem of a tracker, this is has not been implemented and cannot be tested yet.

But an adaptive processing scheme may work, and an acceleration scheme like the scheme explained for bistatic velocities may be developed. This requires an adaptive Doppler shift for each of the tracked targets in the correlation, and may increase the (S/N) with same gain as the scheme explained for range walk.
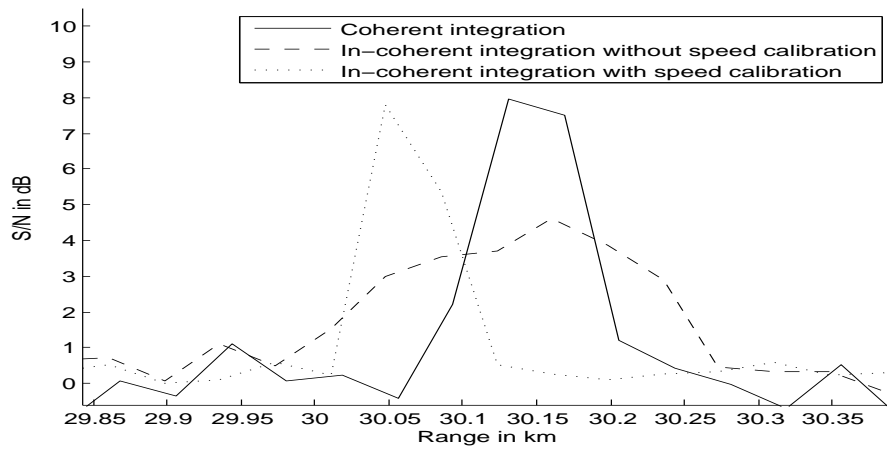
(a) Cross section in range for integration time $T_I = 0.52s$ and $N = 8$
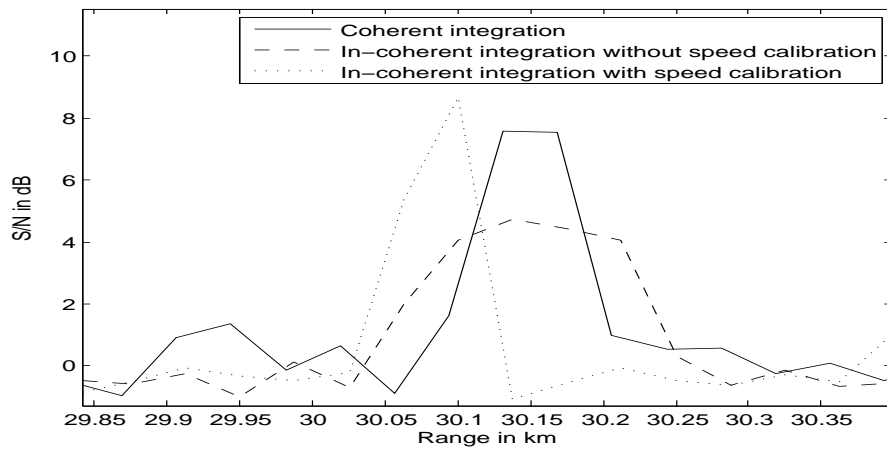
(b) Cross section in range for integration time $T_I = 0.52s$ and $N = 4$
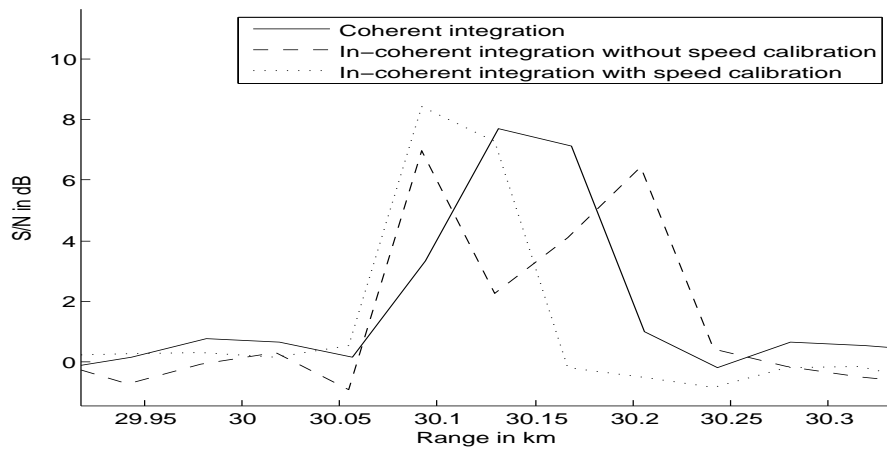
(b) Cross section in range for integration time $T_I = 0.52s$ and $N = 2$

Figure 8.1: Cross section in range for the same coherent integration time, but for different non-coherent integration intervals, for a simulated target

(a) Cross section in range for integration time $T_I = 0.52s$ and $N = 8$
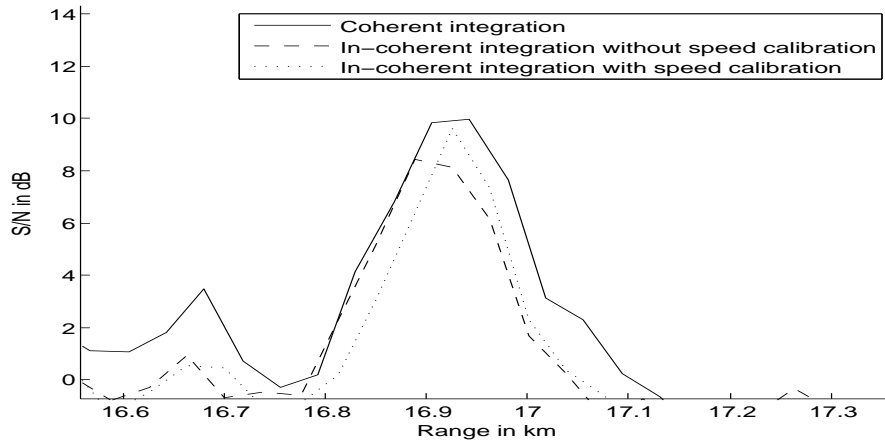

(b) Cross section in range for integration time $T_I = 0.52s$ and $N = 4$
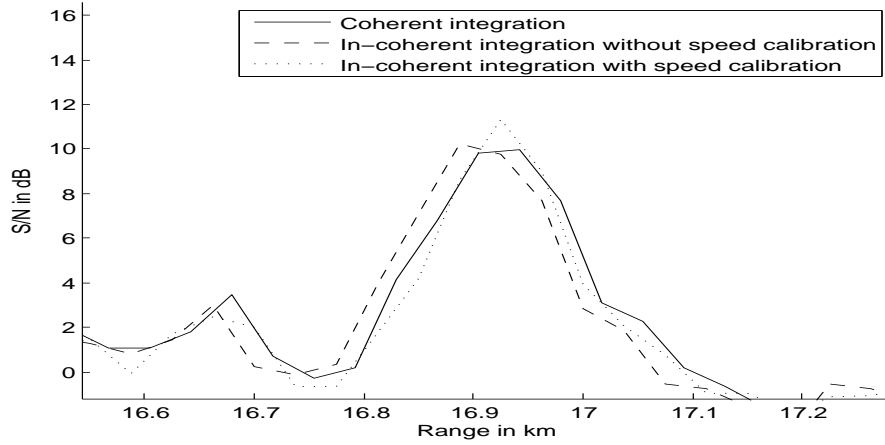

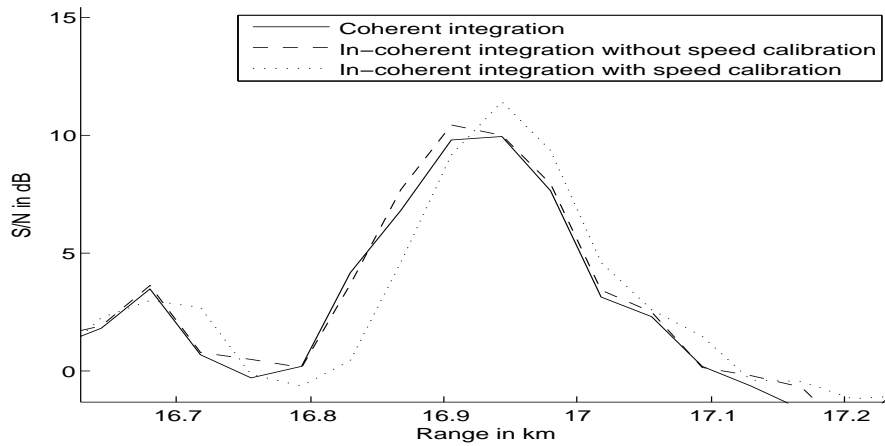(b) Cross section in range for integration time $T_I = 0.52s$ and $N = 2$

Figure 8.2: Cross section in range for the same coherent integration time, but for different non-coherent integration intervals, for a real target
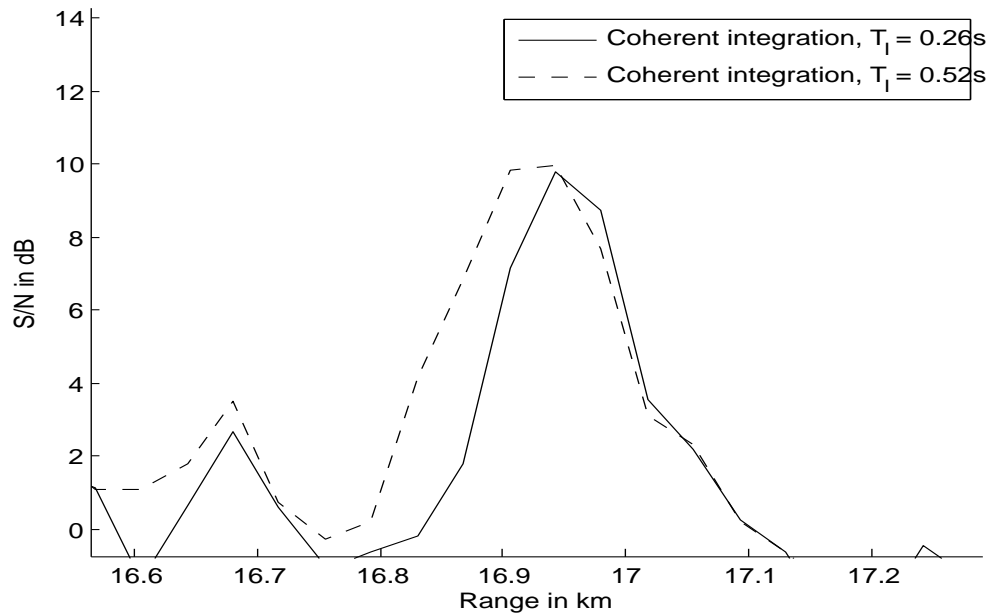
(a) Cross section in range for coherent integration with integration times $0.26s$ and $0.52s$, showing no gain in (S/N) when doubling the integration time.
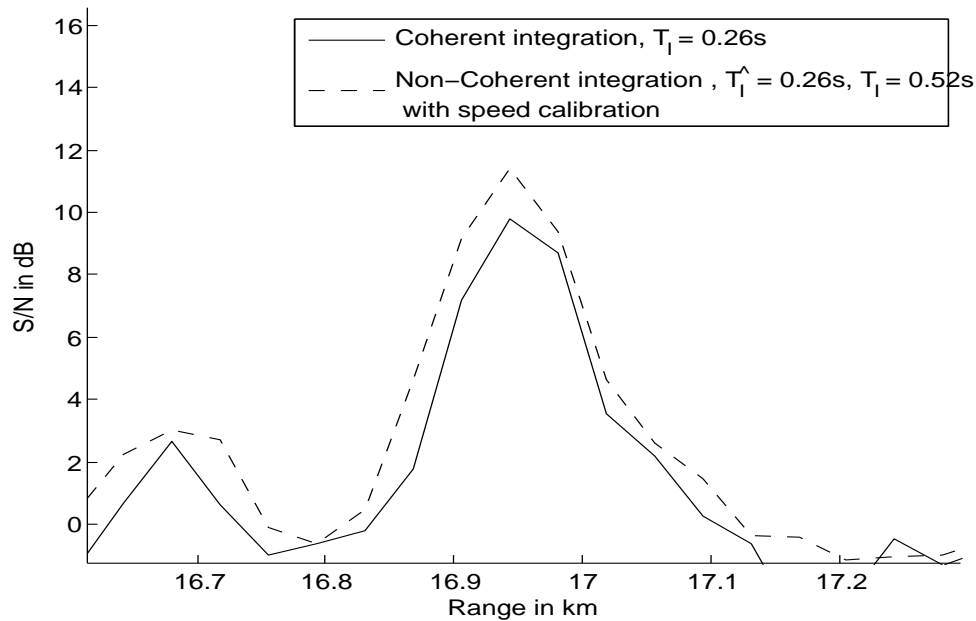
(b) Cross section in range for coherent integration with integration times $0.26s$ and non-coherent integration with speed calibration, showing an $1.5dB$ gain in (S/N) when doubling the integration time.

Figure 8.3: Figure shows the advantage non-coherent integration with speed calibration has over coherent integration when range walk is occurring

9 Conclusions

Most existing PCL/PBR systems are based on FM broadcasts, however due to the introduction of digital TV and radio, digital radio and TV based PCL/PBR systems are currently under analysis. They have many promising properties, although problems may arise. Especially digital TV signals have a large bandwidth resulting in fine range resolution. The fine resolution combined with high velocity targets such as in air surveillance may give rise to problems such as range and Doppler walk. Range walk occurs when the target moves through several range bins during the integration time, and Doppler walk occurs when the target moves through several Doppler bins during the integration time.

PBR is a passive and bistatic radar, which means that the transmitter and receiver are separated in space and the transmitter is non-cooperative. The introduction defines the notation of PBR, and section 1 defines bistatic radar. By setting the parameter β and L to zero and $R_T = R_R = R$ in the bistatic radar equations, you get the monostatic radar equations. Bistatic radar systems are theoretically more complex because of the geometry. Since the transmitters are non-cooperative, the waveform and transmitter placements are not optimal in the sense of a radar system, but optimal for digital TV broadcast.

The DVB-T waveform and transmitter network was shown in section 2. The waveform is expected to be better suited for radar applications than analogue TV due to the stable and large bandwidth. The autocorrelation (see figure 2.3) shows the typical "thumbtack" ambiguity in zero Doppler and range which resembles what a random process produces. However several ambiguities in non-zero Doppler and range were also recognized in the autocorrelation. These arise due to the insertion of deterministic components in the signal. The components were analyzed in section 2.2. Since the non-zero ambiguities are stationary and possible to estimate, they may be removed using a filter.

The processing was done in MATLAB, and the AF was used in the range Doppler processing. Section 4.1 defines the AF and how it was implemented. Range and Doppler walk were defined in sections 4.3 and 4.4. They are effects caused by large bandwidth and long integration times, accompanied with large bistatic velocities and accelerations. They occur when the target moves through several range and/or Doppler bins during signal integration.

A simulator was implemented to analyze the potential problems of range and Doppler walk. Range and Doppler walk are as mentioned a consequence of the large bandwidth and long integration time from using DVB-T as non-cooperative sources of illumination in a PBR system. The simulator was implemented in MATLAB (see section 5.1). The signal generator was implemented to follow the DVB-T standard, and the targets were given a constant bistatic acceleration and/or velocity during the integration interval. Range and Doppler

walk were analyzed (see sections 5.3 and 5.4), and the simulations showed that they may pose problems for a DVB-T based PBR system. Range and Doppler walk widened the target response in the correlation, and lowered the (S/N) gain expected when increasing the coherent integration time.

In order to see whether the problems were seen in a real system, the experimental setup was used to produce real life data. Section 6.2 defined the two PBR setups, and sections 6.3 and 6.4 analyzed those. The setup using Kongsvinger was chosen based on low DSI, high powered transmitter and preferable geometry with respect to the approach at Gardermoen airport. Most of the datasets used to analyze range and Doppler walk were from this setup.

Datasets containing targets experiencing range and Doppler walk were analyzed (see section 7.1 for range walk and section 7.2 for Doppler walk), and the results from the simulations were backed up by experimental results. Range and Doppler walk had the effect of widening the target response, and lowering the gain in (S/N) as showed in the simulation (see sections 5.3 and 5.4). Doppler walk was a rare phenomenon since Doppler walk requires non zero bistatic acceleration and no maneuvering targets were analyzed. For maneuvering targets, Doppler walk may impose a real problem on probability of detection and tracking.

Range walk occurs because of large bistatic velocity compared to integration time and bandwidth (see (4.4) for limit on integration time versus bistatic velocity and signal bandwidth). To limit the effects of range walk, section 8.1 analyzed a method to center the energy by using the Doppler information and non-coherent integration. By using Doppler information to calibrate the speed and noncoherent integration, we can get the gain of noncoherent integration without range walk (seee figure 8.3).

Doppler walk occurs because of large bistatic accelerations. An adaptive processing scheme (see section 8.2) could decrease the effects of Doppler walk, but it requires an estimate of the bistatic acceleration. It can therefore only be implemented after target detection and an acceleration estimate is done. The reason for this is that no second degree information is estimated in the integration process. This was not analyzed further in this work, since no target detector and tracker were implemented.

The effects of range and Doppler walk on a DVB-T based PBR system have been analyzed in this work, and it was shown that they impose potential problems for the implementation of DVB-T based PBR. Range and Doppler walk were proven to cause problems for the probability of detection through simulations and this was backed by experimental data. A method to reduce the effects of range walk is presented, and showed a gain in (S/N) ratio performance especially when correlating high velocity targets.

References

[1] Mikhail Cherniakov. *Bistatic Radars: Emerging Technology.* 2008.

[2] ETSI. Digital video broadcasting (dvb); framing structure, channel coding and modulation for digital terrestial television. 300 744 v1.5.1, 2004-11.

[3] H. D. Griffiths. From a different perspective: Principles, practice and potential of bistatic radar. *IEE 2003, Radar 2003*, 2003.

[4] K. E. Olsen, T. Johnsen, S. Johnsrud. Details of the signal processing, simulations and results from the Norwegian multistatic radar DiMuRa. *Proceedings of the IEEE Waveform Diversity and Design Conference*, February 2006.

[5] Nadav Levanon. *Radar Principles.* 1988.

[6] Lora G. Weiss. Wavelets and wideband correlation processing. *IEEE Signal Processing Magazine*, 11(1):13–32, Jan 1994.

[7] Nicholas J. Willis. *Bistatic Radar, 2nd Edition.* 1995.

[8] Nicholas J. Willis and Hugh D. Griffiths. *Advances in Bistatic Radar.* 2007.

Abbreviations

S/N	-	Signal to Noise ratio
DSI	-	Direct Signal Interference
PBR	-	Passive Bistatic Radar
PCL	-	Passive Coherent Location
DVB-T	-	Digital Video Broadcast - Terrestrial
QPSK	-	Quadratic Phase Shift Keying
QAM	-	Quadrature Amplitude Modulation
OFDM	-	Orthogonal Frequency Division Multiplexing
FFT	-	Fast Fourier Transform
IFFT	-	Inverse Fast Fourier Transform
DFT	-	Discrete Fourier Transform
IDFT	-	Inverse Discrete Fourier Transform
UHF	-	Ultra High Frequency
SFN	-	Single Frequency Network
AF	-	Ambiguity Function
ADSB	-	Automatic Dependent Surveillance - Broadcast
DQD2	-	Dual Quadratic Demodulator 2
ADC	-	Analog to Digital Converter
dB	-	Decibel
IMU	-	Inertial Measurement Unit
GPS	-	Global Positioning System
FM	-	Frequency Modulation
MPEG	-	Moving Picture Experts Group
LAN	-	Local Area Network
USB	-	Universal Serial Bus
RCS	-	Radar Cross Section
DTED	-	Digital Terrain Elevation Data
FFI	-	Forsvarets Forskningsinstitutt

Appendix A   Problem Description

Passive Coherent Location (PCL) is a radar that exploits the available broadcast transmitter's energy in order to detect and track targets, deploying only a (passive) receiver. The FM radio has proven to be a well suited broadcast system for PCL operations, and the most advanced FM radio based PCL systems are aiming at operational status. Digital Video Broadcast - Terrestrial (DVB-T) is a newer television broadcast system that is well suited for PCL applications. The DVB-T system is just declared fully operational in Norway, and within short time the only option for watching terrestrial broadcasted television. There are substantial differences between the two waveforms; FM radio is a Frequency Modulated (FM) waveform, which is highly dependent on the information signal, while the DVB-T is using an Orthogonal Frequency-Division Waveform (OFDM), which due to the inherent coding is independent of the information signal.

The FM radio system broadcasts several channels separated in frequency, where each channel is assigned a 200kHz band. The DVB-T channel has a bandwidth of 8MHz, and within this band there are several coded TV channels. PCL systems are utilizing long integration times, up to one second, and the relatively high bandwidth of the DVB-T signal raises issues with respect to targets moving through range resolution cells, as well as manoeuvring targets sliding through Doppler resolution cells. Both these issues can results in missing detections and wrong tracking if not properly dealt with.

FFI has developed the hardware for an experimental Passive Bistatic Radar (PBR) system to be used with FM radio and DVB-T broadcasters. A PBR system can be regarded as a subset of the PCL system, which basically consists of several PBR systems working togehter. The work shall focus on the DVB-T part of the PBR.

The work shall consist of a DVB-T PBR background survey, a theoretical and/or practical formulation of the issues of targets moving through bistatic range and/or Doppler cells. The candidate will have to implement the necessary processing schemes in order to produce range- Doppler plots of targets, as well as choose a proper geometry for real life data collection, and finally collect suitable targets of opportunity data (no dedicated targets will be made available). The results of the real life target data analysis should be backed by proper theoretical simulations. The focus of the work shall be on DVB-T PBR issues of range and Doppler migration of targets (of opportunity) in resolution cells due to high signal bandwidth and long integration time.